

Contents lists available at [ScienceDirect](https://www.sciencedirect.com)

# International Journal of Applied Earth Observations and Geoinformation

journal homepage: [www.elsevier.com/locate/jag](http://www.elsevier.com/locate/jag)

## Bathymetry retrieval from CubeSat image sequences with short time lags

Milad Niroumand-Jadidi<sup>a,\*</sup>, Carl J. Legleiter<sup>b</sup>, Francesca Bovolo<sup>a</sup><sup>a</sup> Digital Society Center, Fondazione Bruno Kessler, Via Sommarive, 18 I-38123 Trento, Italy<sup>b</sup> U.S. Geological Survey, Integrated Modeling and Prediction Division, Golden, CO 80403, USA

### ARTICLE INFO

#### Keywords:

CubeSats  
PlanetScope  
Bathymetry  
Image averaging  
Short time lag  
Machine learning  
River  
Depth

### ABSTRACT

The rapid expansion of CubeSat constellations could revolutionize the way inland and nearshore coastal waters are monitored from space. This potential stems from the ability of CubeSats to provide daily imagery with global coverage at meter-scale spatial resolution. In this study, we explore the unique opportunity to improve the retrieval of bathymetry offered by CubeSats, specifically those of the PlanetScope constellation. The orbital design of the PlanetScope constellation enables the acquisition of image sequences with short time lags (from seconds to hours). This characteristic allows multiple images to be captured during a short period of steady bathymetric conditions, especially in dynamic environments like rivers. We hypothesize that taking the ensemble mean of a CubeSat image sequence can enhance bathymetry retrieval compared to standard single-image analysis. Along with the existing optimal band ratio analysis (OBRA) algorithm, we also use a new neural network-based depth retrieval (NNDR) technique to infer bathymetry from both individual and time-averaged images. The two methodologies are evaluated using field data from five different river reaches with depths up to 15 m and both top-of-atmosphere (TOA) radiance and bottom-of-atmosphere (BOA) surface reflectance PlanetScope data products. Despite low spectral resolution and concerns about the radiometric quality of CubeSat imagery, accuracy assessment based on in-situ comparisons indicates the potential ( $0.52 < R^2 < 0.7$  for the NNDR method) of PlanetScope imagery to retrieve depths up to  $\sim 10$  m in clear water conditions. The proposed image averaging consistently improves bathymetry retrieval over single image analysis. The NNDR technique was found to outperform OBRA, illustrating the importance of leveraging all spectral bands through machine learning approaches. TOA data provided more robust bathymetry results than BOA data for the OBRA technique, but the NNDR technique was minimally impacted by the type of data product.

### 1. Introduction

With recent advances in the development of CubeSat constellations, remote sensing of inland and nearshore coastal waters has entered a revolutionary era (Cooley et al., 2017; Niroumand-Jadidi et al., 2020b; Niroumand-Jadidi and Bovolo, 2021). This progress has been enabled by the capability of CubeSat constellations to capture imagery with unprecedented daily coverage and meter-scale resolutions. This unique characteristic is made possible by fleets consisting of a large number of small satellites. CubeSats thus fill the persistent gap between spaceborne imagers that acquire data with high temporal resolution but very coarse pixels e.g., Moderate Resolution Imaging Spectroradiometer (MODIS) (Salomonson et al., 2006) and those with much better spatial resolution but far less frequent coverage like WorldView (Wilson et al., 2022). The meter-scale spatial resolution of CubeSats creates the possibility of monitoring even small inland water bodies like river channels, for which

the spatial resolution of common satellites (e.g., Landsat-8 and Sentinel-2) is too coarse (Mansaray et al., 2021). In addition, the daily revisit frequency improves the likelihood of acquiring cloud-free images and allows the temporal dynamics of biophysical attributes like water quality and bathymetry (depth of water measured from the water surface down to the streambed) to be captured (Vanhellemont, 2019). The combination of high spatial and temporal resolution and the potential for near-real-time remote sensing could greatly facilitate advances in aquatic science and management.

PlanetScope is the most prominent CubeSat constellation, with >180 CubeSats, known as Doves, currently in orbit (Planet Team, 2021). This constellation provides daily imagery of the entire landmass of Earth with  $\sim 3$  m spatial resolution. Moreover, PlanetScope data are available at no cost for research purposes. The application of PlanetScope imagery to aquatic systems has recently received increasing research attention. For instance, the bathymetry of coastal areas has been retrieved based

\* Corresponding author.

E-mail address: [mniroumand@fbk.eu](mailto:mniroumand@fbk.eu) (M. Niroumand-Jadidi).

<https://doi.org/10.1016/j.jag.2022.102958>

Received 10 January 2022; Received in revised form 13 July 2022; Accepted 2 August 2022

Available online 11 August 2022

1569-8432/© 2022 The Authors. Published by Elsevier B.V. This is an open access article under the CC BY-NC-ND license (<http://creativecommons.org/licenses/by-nc-nd/4.0/>).

on empirical and semi-empirical models using PlanetScope imagery (Gabr et al., 2020; Li et al., 2019; Poursanidis et al., 2019). The PlanetScope data provided promising bathymetry and total suspended matter (TSM) retrievals in the Venice lagoon using a physics-based approach Niroumand-Jadidi et al., 2020b. Some studies also demonstrated the potential of PlanetScope imagery in retrieving water quality indicators (e.g., chlorophyll-a and turbidity), as well as detection of algal blooms (Mansaray et al., 2021; Niroumand-Jadidi and Bovolo, 2021; Vanhellemont, 2019).

Despite the unparalleled advantages of Planet Doves in terms of spatial and temporal resolution, low spectral resolution (four bands) and concerns about the radiometric quality and consistency among multiple platforms can limit aquatic applications (Cooley et al., 2017; Niroumand-Jadidi et al., 2020b). The issue of low spectral resolution is more pronounced in optically complex waters, where narrower spectral bands might be required to resolve diagnostic absorption features (Giardino et al., 2019). The radiometric quality of optical imagery also plays a key role in deriving biophysical parameters in aquatic systems (Niroumand-Jadidi et al., 2021). This is because a relatively small fraction of the downwelling solar irradiance is reflected from within the water body or from the bottom due to the strong attenuation of light by pure water (Giardino et al., 2019; Toming et al., 2016). As a result, the radiometric sensitivity of satellite sensors tends to be insufficient to detect subtle variations in water-leaving radiance, as the signal-to-noise ratio (SNR) is reduced by artifacts associated with the atmosphere and sun glint (Moses et al., 2017). Planet Doves capture images with a 12-bit dynamic range that is similar to that of standard sensors onboard Sentinel-2 and Landsat-8 (Mandanici and Bitelli, 2016). The concern regarding the possibly lower radiometric quality stems from the fact that CubeSats, by definition, carry small and inexpensive sensors that might not achieve the same quality (i.e., SNR) and consistency as more typical, much larger satellite sensors (Cooley et al., 2017; Houborg and McCabe, 2016).

In this study, we focus on bathymetry retrieval and exploit a unique characteristic of the PlanetScope constellation that remains largely unexplored. Although many studies highlight the daily acquisitions provided by Planet Doves, the revisit frequencies are actually even better: sub-daily. The constellation design of PlanetScope allows imaging the Earth's surface with short time lags, ranging from seconds to a few hours between images. The Planet Doves are deployed in two near-polar orbits with opposite inclinations at an altitude of  $\sim 475$  km, allowing image acquisitions from both ascending and descending orbits. The swaths of subsequent CubeSats in each orbit overlap in the across-track direction by a few kilometers. These swath overlaps allow for the acquisition of pairs of images with a time lag of about 90 s. Acquisitions from both ascending and descending orbits of the PlanetScope constellation yield other time lags in the range of a few minutes to a few hours (Kääb et al., 2019; Roy et al., 2021). To date, little attention has been paid to this particular attribute of the PlanetScope constellation in aquatic applications. To our knowledge, the only study to capitalize upon this capability focused on estimating water surface velocities by tracking river ice floes over the short (90 s) time lag between images captured by subsequent Planet Doves (Kääb et al., 2019). Thus, a need clearly exists to further examine and unlock the potential of short time lag CubeSat image sequences in general and specifically in the context of aquatic applications.

In this study, we examine ensemble-averaging of Dove acquisitions with short time lags as a means of improving bathymetry retrieval. The idea is built upon the recent work of Legleiter and Kinzel (2021a) on inferring bathymetry from averaged river images (IBARI). IBARI provided improved depth retrieval in a clear-flowing river by using time-averaged images derived from videos rather than single image frames. This method mitigated the noise present in single images due to reflectance from an irregular water surface (i.e., sun glint). Although IBARI originally was developed for analyzing helicopter-based videos, we hypothesize that this framework could be extended to depth retrieval

from space by exploiting short time lag images from the PlanetScope constellation. Preserving short time lags among images is important in mapping bathymetry to ensure that water depth remains steady over the acquisition period. This is of particular importance in fluvial systems where the streamflow and associated water level can vary significantly over time. Similarly, in coastal waters, the depth can be influenced by tidal effects and inland inflows. Moreover, short time lags among acquisitions maximize the homogeneity of images in terms of atmospheric and illumination conditions, which is important for creating an internally consistent ensemble.

Various spectrally-based methods for inferring bathymetry from optical imagery can be categorized into two main groups: empirical (regression-based) and physics-based approaches (Dekker et al., 2011; Hodúl et al., 2018; Niroumand-Jadidi et al., 2020a, 2018). The empirical bathymetry retrieval is based on training a regression model using in-situ depth samples (Legleiter et al., 2009; Lyzenga, 1978; Niroumand-Jadidi and Vittori, 2016; Shintani and Fonstad, 2017). Physics-based models rely on comparing the observed (image) spectra with radiative transfer simulations that model the interaction of light with the water surface, water column, and substrate (Gege, 2014; Mobley, 1994; Niroumand-Jadidi et al., 2020b). The original IBARI is based on an empirical bathymetry method called optimal band ratio analysis (OBRA) developed by Legleiter et al. (2009). OBRA is based on the widely used band ratio model (Stumpf et al., 2003) and examines all possible band combinations to identify the optimal pair of bands (Legleiter et al., 2009). In this study, in addition to standard OBRA, we propose an empirical machine learning-based method called neural network depth retrieval (NNDR) to examine the effectiveness of averaging Planet Dove image sequences with short time lags.

Machine learning approaches like support vector machines and random forests have provided promising results when used to retrieve coastal bathymetry (Tonion et al., 2020). An NN-based empirical model was also tested for bathymetry retrieval in a harbor environment using Landsat-8 imagery (Makboul et al., 2017). More recently, a convolutional NN (CNN) model was used to estimate water depths from aerial imagery (Mandlbürger et al., 2021). A comprehensive review of empirical approaches for depth retrieval, including machine learning techniques, is presented by Mandlbürger et al. (2021). However, machine learning-based models remain understudied in bathymetry retrieval, particularly in fluvial systems (Legleiter and Harrison, 2019a). Although the main objective of this study is not to develop a new bathymetry retrieval method, we use NNDR to examine the impact of using a machine learning approach rather than OBRA for depth retrieval from time-averaged imagery. We explore the utility of NNs for inferring bathymetry as they can learn complex and non-linear relations between predictors (spectral bands) and the response parameter (water depth) (Murtagh, 1991). Furthermore, NNs can identify and exploit the most informative features from all of the original spectral bands, with no need for extraction of features in advance (Murtagh, 1991; Shaheen et al., 2016).

We pursue the following objectives: (i) introduce a framework for analyzing ensembles of PlanetScope images acquired with short time lags, (ii) examine the effectiveness of ensemble averaging in improving bathymetry retrieval compared to the typical single-frame analysis, (iii) develop a machine learning-based bathymetry method (i.e., NNDR) and examine its effectiveness compared to standard OBRA when applied to single-frame and time-averaged images, and (iv) evaluate the depth retrieval accuracies derived from both top-of-atmosphere (TOA) radiance and bottom-of-atmosphere (BOA) surface reflectance data products from the PlanetScope constellation. The manuscript is structured as follows. The methodology of the study is presented in Section 2. Section 3 introduces our case studies and associated imagery and in-situ data. Experimental results and discussion are provided in Sections 4 and 5, respectively. Finally, concluding remarks and an outlook for future work are presented in Section 6.

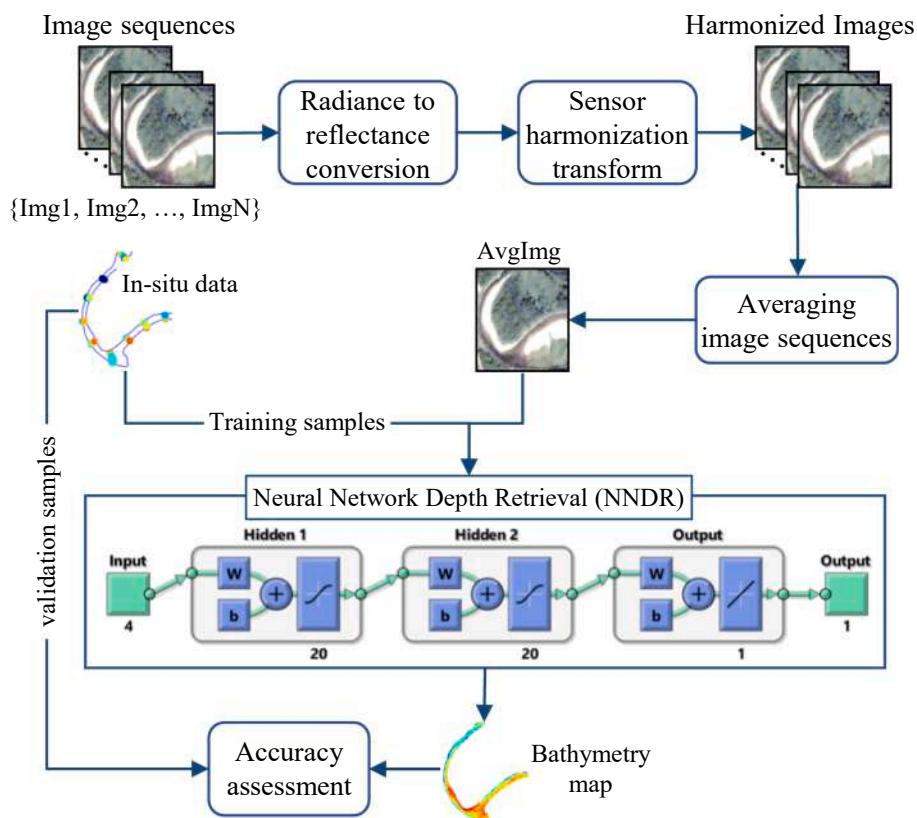


Fig. 1. Workflow of the proposed approach for bathymetry retrieval based on averaging image sequences acquired by CubeSats. The labels  $w$  and  $b$  refer to weights and biases, respectively.

## 2. Methods

Most studies involving CubeSat data analysis emphasize the advantages of daily acquisitions that are more likely to yield cloud-free images of a given location. However, less attention has been paid to sub-daily imagery that could provide new opportunities, particularly in aquatic applications. In this study, we assume that images with short time lags can offer multiple observations of bathymetric conditions that remain steady over the duration of the image sequence. Thus, we hypothesize that ensembling the short time lag images can mitigate image noise and thus improve bathymetry retrieval. This approach is built upon the IBARI framework (Legleiter and Kinzel, 2021a), in which the ensemble consisted of video frames acquired from a helicopter platform. However, we note several key distinctions in applying an IBARI-like method to spaceborne CubeSat imagery rather than airborne videos. The spatial resolution of CubeSat data is significantly ( $\sim 20$  times) lower than the helicopter images from Legleiter and Kinzel (2021a). The number of images in a CubeSat sequence is limited to only a few (most often two) frames, whereas a video provides tens or hundreds of frames over a few seconds. In this study, we explore the ensembling of CubeSat image sequences as a means of improving bathymetry retrieval.

We employ both TOA radiance and BOA surface reflectance data products from Planet Doves. The first step for ensembling the CubeSat images is TOA radiance to TOA reflectance conversion. This step is required only for the TOA radiance products to account for changes in illumination and sensor viewing angles. Note that the view angle of PlanetScope data currently varies only within a few degrees from nadir (Ghuffar, 2018). All of the data used in this study were near nadir ( $<5^\circ$ ) with only slight variations in view angle between sub-daily acquisitions. Another important step is the radiometric harmonization of images acquired by different generations of PlanetScope sensors. The harmonization transforms values from the latest PlanetScope sensors (namely

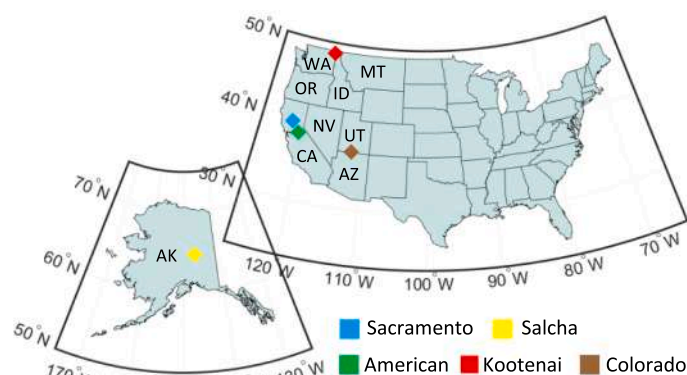
PS2.SD and PSB.SD) to match those of the early PlanetScope satellites (PS2). The harmonization transform parameters are provided in the metadata accompanying the imagery and consist of multiplicative coefficients for each band. This transform mitigates radiometric inconsistencies among image sequences captured by different sensors. We then perform image-averaging on the harmonized reflectance data, either TOA or BOA. The averaging is performed over time on a per-pixel basis. Note that because the Dove data are orthorectified, pixels correspond to one another spatially throughout an image time series (Planet Team, 2021). Denoting the feature vector of reflectances at different wavelengths  $\lambda$  of an image pixel acquired at time  $t$  as  $R_t(\lambda)$ , the time-averaged image value  $\bar{R}(\lambda)$  can be derived for a sequence consisting of  $T$  images as follows:

$$\bar{R}(\lambda) = \frac{\sum_{t=1}^T R_t(\lambda)}{T} \quad (1)$$

A minimum of two images is required to perform the time averaging. The number of images  $T$  can be increased depending on the availability of short time lag images. Moreover, if the bathymetry remains steady over a longer period of time, additional Dove images from days prior to and following the image acquisition also can be incorporated into the ensemble.

To examine the effectiveness of ensemble-averaging Dove acquisitions for inferring bathymetry, we also propose a neural network-based depth retrieval (NNDR) technique, which we implemented using the Deep Learning Toolbox of the MATLAB software package (MATLAB, 2022). NNDR is a multilayer perceptron (Murtagh, 1991) with two hidden layers that takes the original bands of the PlanetScope data (i.e., four spectral features) as input and provides the water depth as output. In our analyses, each hidden layer consists of 20 neurons. The numbers of hidden layers and neurons are defined through a tuning step by varying these parameters. The same architecture provided stable results





(a) Location of studied river reaches. Map source: MATLAB (2022) basemaps.

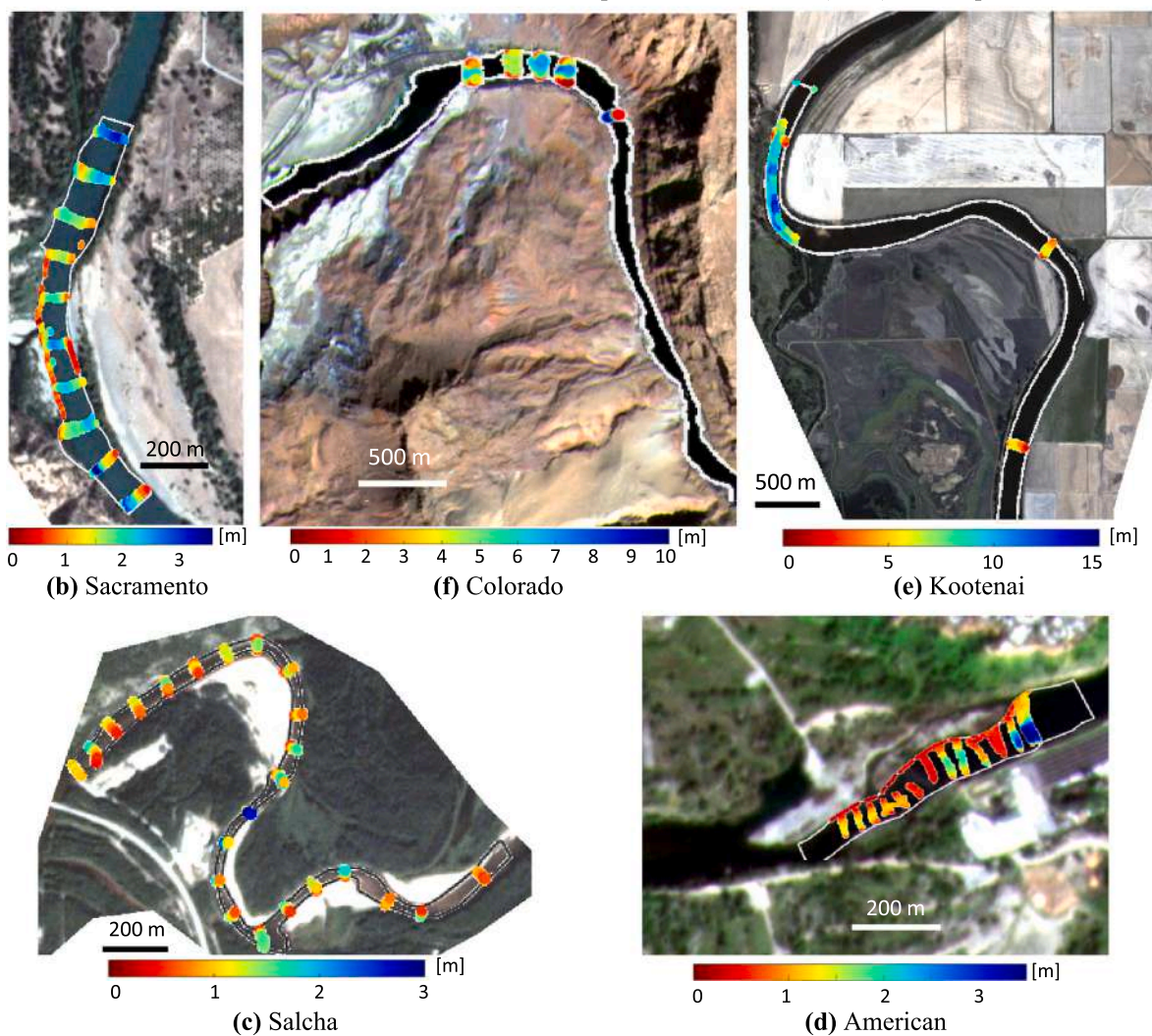


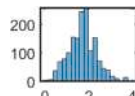
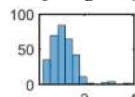
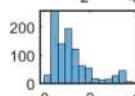
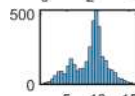
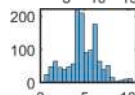
Fig. 2. The location of the case study river reaches on the U.S. map and associated true color composites of PlanetScope imagery. The in-situ bathymetry samples are superimposed with colors showing the water depth. Imagery © 2022 Planet Labs Inc.

for the different case studies presented herein. We divided the in-situ data into training, test, and validation subsets based on a common random selection approach (Legleiter et al., 2014; Pontoglio et al., 2020). The training subset (35 % of samples) is used for computing the gradient and updating the network weights and biases (Fig. 1). The network uses the test subset (15 % of samples) to monitor the error during the training process. A reduction in the test error normally occurs during the initial phase of training. However, when the network begins to overfit, the error on the validation set increases. The network

parameters (weights and biases) are saved at the minimum of the test set error so as to mitigate the overfitting problem and achieve a more generic model. The training is stopped when the test error increases for a specified number of iterations (here set to 6). The training is repeated ten times (with random sample selection from 50 % holdout for training and test), and the average sample depth estimate for these ten replicates is considered the final retrieval. The validity of the model is then assessed based on the validation set (50 % of samples) that is not used during the training phase.

**Table 1**

Characteristics of studied rivers and selected PlanetScope image sequences along with the statistics of available in-situ depth samples.

River and USGS site number	Characteristics	PlanetScope imagery		Gage water level * [m]	In-situ depths [m] distribution	In-situ samples statistics
		ID	Date and time			
<b>Sacramento</b> 11,377,100	Moderately clear, ~110 m wide; single meander bend	Img1	20170913_181326	1.16		N = 1581 Mean = 1.74 m Std = 0.64 m
		Img2	20170913_181552	1.16		
<b>Salcha</b> 15,484,000	Very clear water, ~50 m wide; longer reach with multiple bends	Img1	20190722_210207	2.07		N = 319 Mean = 1.18 m Std = 0.54 m
		Img2	20190723_204419	2.06		
<b>American</b> 11,446,500	Clear water below dam, ~80 m wide; short study reach at a river restoration site	Img1	20201019_180351	2.20		N = 990 Mean = 1.21 m Std = 0.84 m
		Img2	20201019_183224	2.22		
		Img3	20201021_180626	2.21		
<b>Kootenai</b> 12,310,100	Very clear water, ~125 m wide; meandering channel with data from several bends	Img1	20170923_180021	13.93		N = 3805 Mean = 8.77 m Std = 2.62 m
		Img2	20170923_180211	13.93		
<b>Colorado</b> 09,380,000	Clear water below dam, ~100 m wide; short, straight reach	Img1	20210317_172334	2.04		N = 1332 Mean = 4.85 m Std = 1.89 m
		Img2	20210318_173212	2.03		
		Img3	20210319_175930	2.03		

\* The gage water level is the height above an arbitrary datum specific to each gage. For this study, only the difference in water level between image acquisitions is of interest as a means of ensuring that bathymetric conditions were steady.

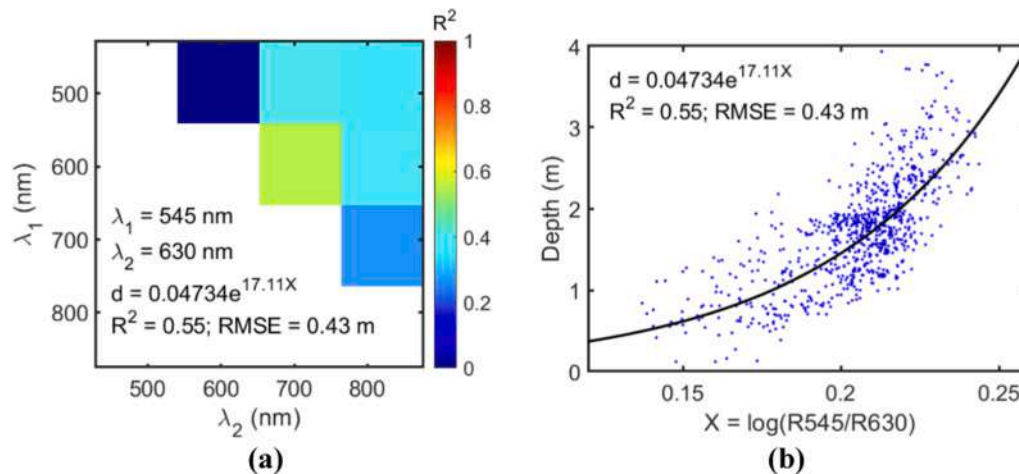


**Fig. 3.** (a) OBRA of time-averaged image for the Sacramento River and (b) associated regression model.

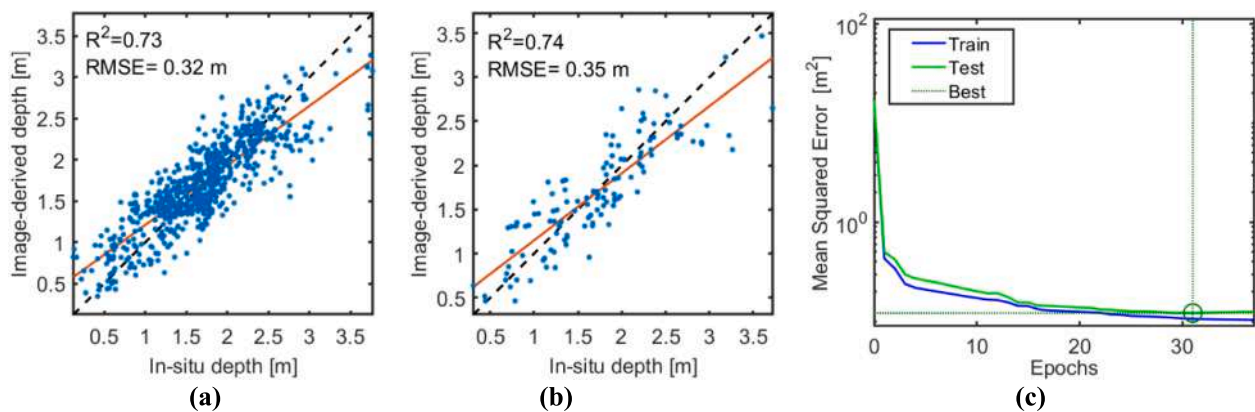


**Fig. 4.** (a) Training and (b) test comparison along with (c) performance of the proposed NNDR at different epochs for bathymetry retrieval from the time-averaged image of Sacramento River.



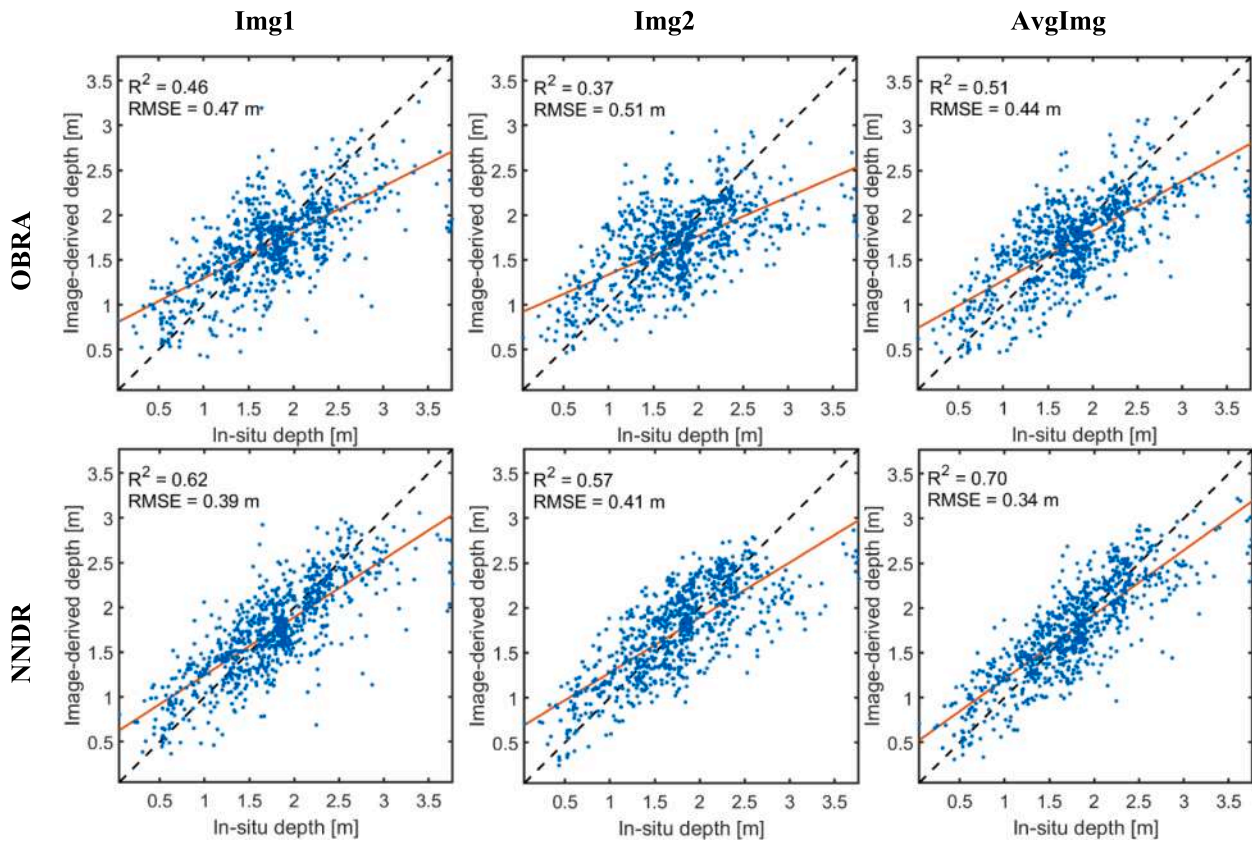


Fig. 5. Validation of depth retrieval from single (Img1 and Img2) and time-averaged (AvgImg) images based on OBRA and NNDR for the Sacramento River.

Table 2

Accuracy statistics of bathymetry retrieval based on OBRA and NNDR considering TOA and BOA single (Img1 and Img2) and time-averaged (AvgImg) images for the Sacramento River. The best performances are indicated by bold font.

		Img1		Img2		AvgImg	
		OBRA	NNDR	OBRA	NNDR	OBRA	NNDR
<b>R<sup>2</sup></b>	TOA	0.46	0.62	0.37	0.57	0.51	<b>0.70</b>
	BOA	0.53	0.63	0.46	0.55	0.61	<b>0.68</b>
<b>RMSE [m]</b>	TOA	0.47	0.39	0.51	0.41	0.44	<b>0.34</b>
	BOA	0.44	0.39	0.48	0.42	0.40	<b>0.35</b>
<b>NRMSE [%]</b>	TOA	13	10	14	11	12	<b>9</b>
	BOA	12	10	13	11	11	<b>9</b>
<b>MAE</b>	TOA	1.26	1.21	1.28	1.22	1.25	<b>1.19</b>
	BOA	1.24	1.21	1.26	1.22	1.23	<b>1.19</b>
<b>Bias</b>	TOA	<b>0.99</b>	<b>1.01</b>	0.98	1.02	0.99	1.02
	BOA	<b>0.98</b>	<b>1.02</b>	0.97	<b>1.02</b>	<b>0.98</b>	1.02

In addition to the proposed NNDR, we also employ OBRA (Legleiter et al., 2009) as an alternative bathymetric mapping method to investigate the effect of averaging image sequences. OBRA examines all possible log-transformed band ratios of spectral data in training a depth retrieval model. Through regressing depths versus band ratios, the pair of bands that provides the highest coefficient of determination ( $R^2$ ) is identified and selected as the optimal band ratio (Legleiter et al., 2009). The log-transformed band ratio at a given time  $t$  and for the time-averaged image are denoted by  $X_t$  and  $\bar{X}$  in Equations (2) and (3), respectively:

$$X_t = \ln \left[ \frac{R_t(\lambda_1)}{R_t(\lambda_2)} \right], d_t = a_t e^{b_t X_t} \quad (2)$$

$$\bar{X} = \ln \left[ \frac{\bar{R}(\lambda_1)}{\bar{R}(\lambda_2)} \right], \bar{d} = \bar{a} e^{\bar{b} \bar{X}} \quad (3)$$

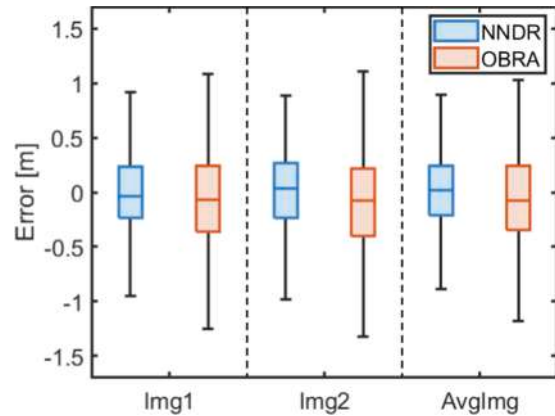


Fig. 6. Errors of bathymetry retrieval from single (Img1 and Img2) and time-averaged (AvgImg) images based on OBRA and NNDR for the Sacramento River.

Note that  $\lambda_1$  and  $\lambda_2$  are the numerator and denominator wavelengths, respectively. In this study, an exponential model is used to estimate depth from either a single image at time  $t$  ( $d_t$ ) or the time-averaged image ( $\bar{d}$ );  $a_t$  and  $b_t$  and  $\bar{a}$  and  $\bar{b}$  represent the coefficients of the exponential relations for the single and time-averaged cases, respectively. The exponential model performed better than the linear or quadratic forms of OBRA used in some previous studies. The exponential formulation has the important advantage of avoiding negative depth estimates in shallow waters, as often occurs when using a linear model (Legleiter, 2021a). To ensure that the analyses are consistent, the validation of OBRA is performed using the same subset of the data as for the validation of NNDR.

We assessed the accuracy of bathymetry retrievals relative to the in-

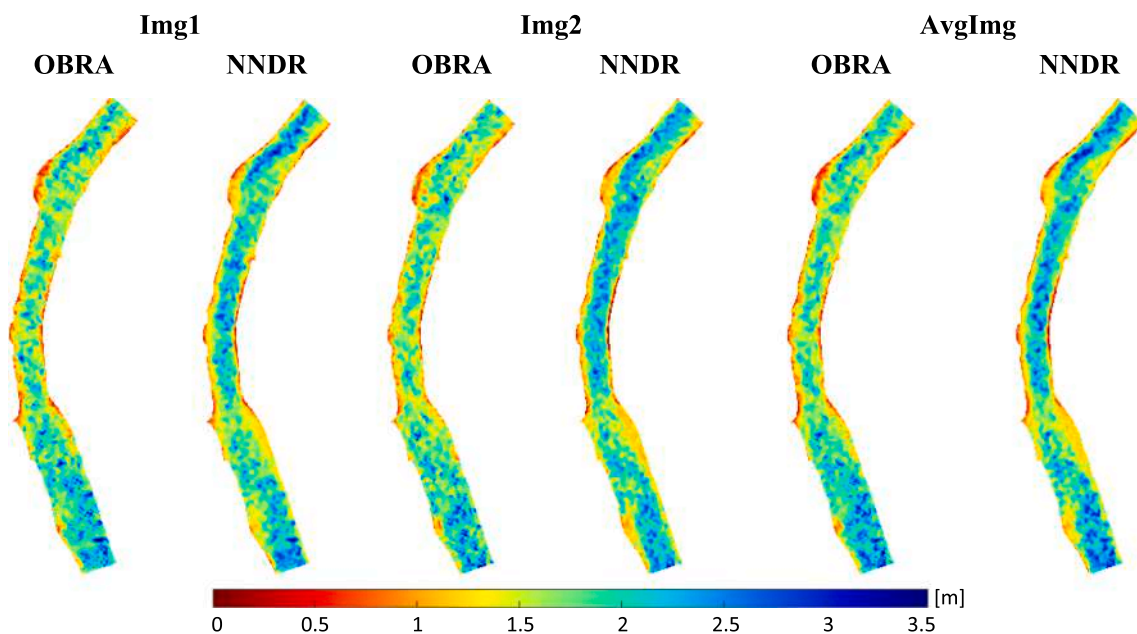


Fig. 7. Bathymetry maps derived from single (Img1 and Img2) and time-averaged (AvgImg) images based on OBRA and NNDR for the Sacramento River.

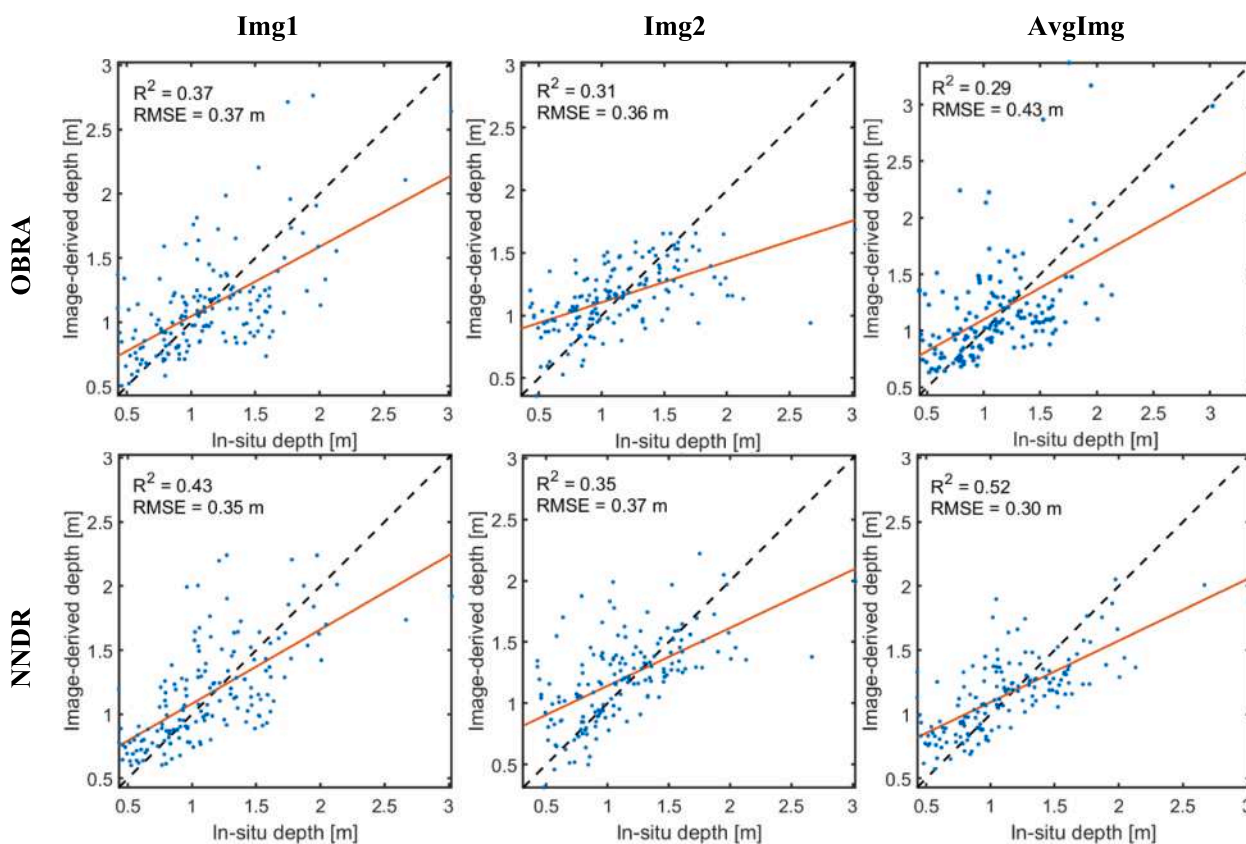


Fig. 8. Validation of depth retrieval from single (Img1 and Img2) and time-averaged (AvgImg) images based on OBRA and NNDR for the Salcha River.

situ data using metrics that quantify the in-situ vs image-derived depth comparisons: coefficient of determination ( $R^2$ ), root mean square error (RMSE), normalized RMSE (NRMSE), bias, and mean absolute error (MAE).  $R^2$  and RMSE are common least-squares metrics used in regression analyses. NRMSE represents the percentage of RMSE relative to the maximum depth. For bias and MAE, we used the recent definition of these metrics in ocean color applications which involves calculating

their values in a log-transformed space to account for the proportionality of the errors with depth (Seegers et al., 2018). The closer the bias to one, the less the estimated depths are biased. Bias > 1 indicates an over-estimation of the retrieved values on average, whereas bias < 1 is an indication of underestimation. For instance, a bias of 1.2 indicates that depth retrievals are on average 1.2 times (20 %) greater than the values measured in the field. MAE always exceeds one and indicates the relative

**Table 3**

Accuracy statistics of bathymetry retrieval based on OBRA and NNDR considering TOA and BOA single (Img1 and Img2) and time-averaged (AvgImg) images for the Salcha River. The best performances are indicated by bold font.

		Img1		Img2		AvgImg	
		OBRA	NNDR	OBRA	NNDR	OBRA	NNDR
$R^2$	TOA	0.37	0.43	0.31	0.35	0.29	<b>0.52</b>
	BOA	0.45	0.45	0.30	0.30	0.43	<b>0.50</b>
RMSE [m]	TOA	0.37	0.35	0.36	0.37	0.43	<b>0.30</b>
	BOA	0.38	0.39	0.44	0.44	0.40	<b>0.35</b>
NRMSE [%]	TOA	12	12	12	12	14	<b>10</b>
	BOA	13	13	15	15	13	<b>12</b>
MAE	TOA	1.28	1.26	1.27	1.28	1.30	<b>1.23</b>
	BOA	1.26	1.26	1.31	1.31	1.29	1.27
Bias	TOA	1.01	1.05	1.07	1.09	1.06	1.07
	BOA	1.04	1.07	<b>1.02</b>	1.06	1.05	1.09

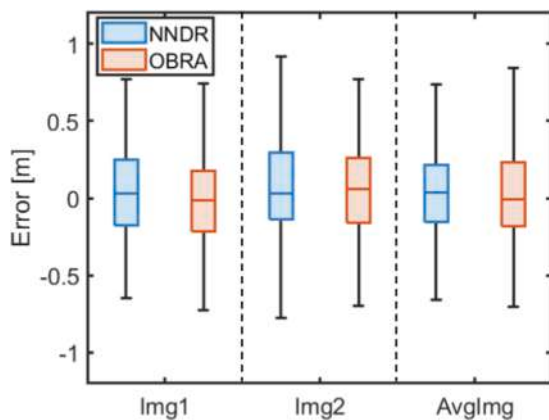


**Fig. 9.** Errors of bathymetry retrieval from single (Img1 and Img2) and time-averaged (AvgImg) images based on OBRA and NNDR for the Salcha River.

error of depth retrieval. Both bias and MAE are unitless. For a total number of  $n$  estimated values  $E_i$  with associated field measured values  $O_i$ , the accuracy metrics can be calculated according to Equations (4) –

8.

$$R^2 = \frac{\sum_{i=1}^n (E_i - \bar{O})^2}{\sum_{i=1}^n (O_i - \bar{O})^2}, \bar{O} = \frac{1}{n} \sum_{i=1}^n O_i \quad (4)$$

$$RMSE = \left( \frac{\sum_{i=1}^n (E_i - O_i)^2}{n} \right)^{1/2} \quad (5)$$

$$NRMSE = \frac{RMSE}{\max(O)} \times 100 \quad (6)$$

$$bias = 10^{\frac{\sum_{i=1}^n \log_{10}(E_i/O_i)}{n}} \quad (7)$$

$$MAE = 10^{\frac{\sum_{i=1}^n |\log_{10}(E_i/O_i)|}{n}} \quad (8)$$

### 3. Case studies and datasets

Five river reaches with relatively clear waters in the US were used as case studies and covered a wide range of water depths. The selected reaches are located on the Sacramento, Salcha, American, Kootenai, and Colorado Rivers. Fig. 2 shows the selected reaches with the associated in-situ depth samples. The Sacramento (Legleiter and Harrison, 2019b), Salcha (Legleiter and Kinzel, 2021b), and American (Legleiter and Harrison, 2022) are shallow reaches (<3.5 m), whereas the Kootenai (Legleiter and Fosness, 2019a) and Colorado (Legleiter et al., 2021) sites include waters up to 15 m deep. Measured turbidities were 3.3 NTU on the Sacramento, 1.09 NTU on the Kootenai, and 0.413 NTU on the Colorado (Legleiter and Harrison, 2019b). Although turbidity data were not collected on the Salcha or American Rivers, the water at these sites was also very clear and presumably had low turbidities similar to those recorded at the other sites. This diverse dataset allowed us not only to test the ensemble-averaging approach to depth retrieval but also broadly evaluate the utility of CubeSat imagery for bathymetric mapping. A brief description of the selected river reaches is provided in Table 1, along with some statistics on the number and distribution of in-situ depth samples. The in-situ data used in this study are available from Legleiter et al. (2021), Legleiter and Harrison (2019a), Legleiter and Harrison,

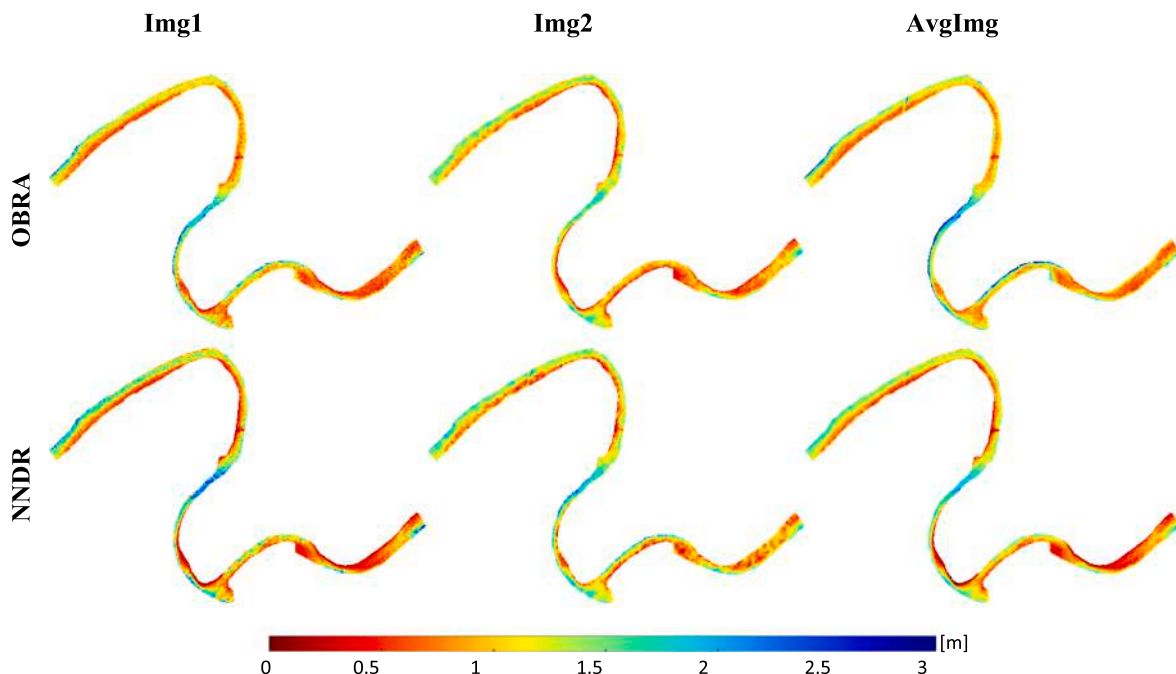


**Fig. 10.** Bathymetry maps derived from single (Img1 and Img2) and time-averaged (AvgImg) images based on OBRA and NNDR for the Salcha River.



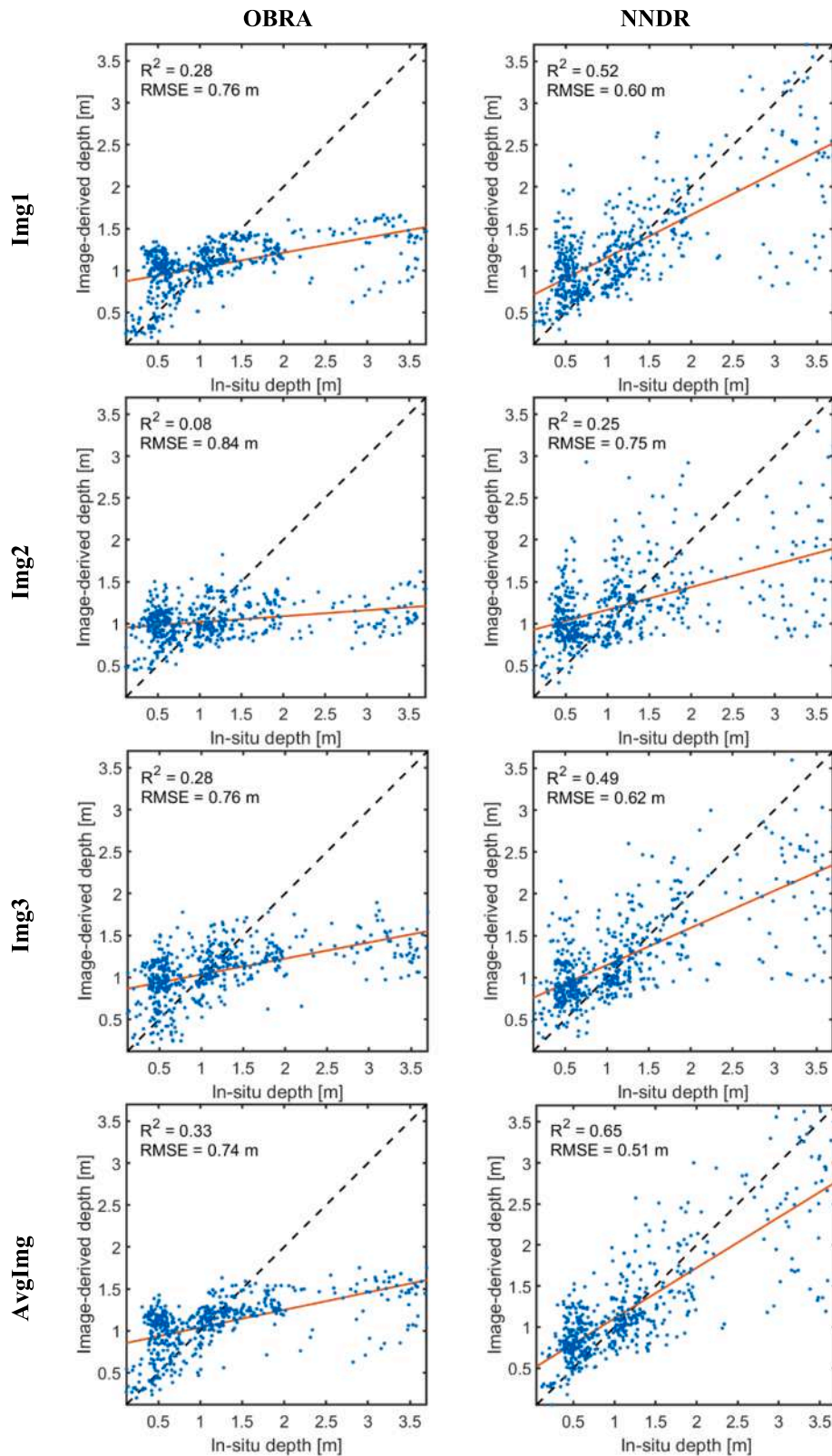


Fig. 11. Validation plots comparing depth retrieval from single (Img1, Img2, and Img3) and time-averaged (AvgImg) images based on OBRA and NNDR for the American River.

2022, and Legleiter and Kinzel, 2021b. Detailed information about the field measurements and characteristics of the river reaches can be found in previous studies conducted on the Sacramento (Legleiter and Harrison, 2019b), Salcha (Legleiter and Kinzel, 2021a), Kootenai (Legleiter

and Fosness, 2019b), Colorado (Legleiter et al., 2021), and American Legleiter and Harrison, 2022 rivers.

We use both TOA radiance and BOA surface reflectance products from Planet Doves. The atmospheric correction of the BOA product is

**Table 4**

Accuracy statistics of bathymetry retrieval based on OBRA and NNDR considering TOA and BOA single (Img1, Img2, and Img3) and time-averaged (AvgImg) images for the American River. The best performances are indicated by bold font.

		Img1		Img2		Img3		AvgImg	
		OBRA	NNDR	OBRA	NNDR	OBRA	NNDR	OBRA	NNDR
$R^2$	TOA	0.28	0.52	0.08	0.25	0.28	0.49	0.33	<b>0.65</b>
	BOA	0.35	0.54	0.10	0.25	0.34	0.52	0.39	<b>0.64</b>
RMSE [m]	TOA	0.76	0.60	0.84	0.75	0.76	0.62	0.74	<b>0.51</b>
	BOA	0.70	0.55	0.81	0.71	0.70	0.57	0.69	<b>0.49</b>
NRMSE [%]	TOA	21	17	23	21	21	17	21	<b>14</b>
	BOA	19	15	22	20	19	16	19	<b>14</b>
MAE	TOA	1.56	1.49	1.70	1.62	1.60	1.51	1.54	<b>1.43</b>
	BOA	1.51	1.45	1.67	1.60	1.57	1.46	1.51	<b>1.42</b>
Bias	TOA	<b>1.07</b>	1.21	<b>1.07</b>	1.21	1.07	1.20	1.08	1.14
	BOA	1.01	1.14	<b>0.99</b>	1.18	0.98	1.10	<b>0.99</b>	1.14

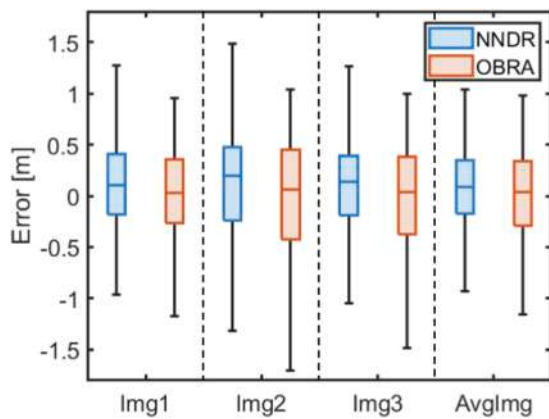


**Fig. 12.** Errors of bathymetry retrieval from single (Img1, Img2, and Img3) and time-averaged (AvgImg) images based on OBRA and NNDR for the American River.

performed by the data provider based on the 6S radiative transfer model considering ancillary data derived from MODIS products (e.g., water vapor, ozone, and aerosol data) (Planet Team, 2021). The spectral resolution of PlanetScope imagery is limited to four bands (455–515 nm, 500–590 nm, 590–670 nm, and 780–860 nm). The acquisition date and time (UTC) of the imagery are listed in Table 1. In some cases, images from adjacent days were also considered if the water level remained steady according to data from a U.S. Geological Survey (USGS) gaging station at the site (U.S. Geological Survey, 2022; Table 1).

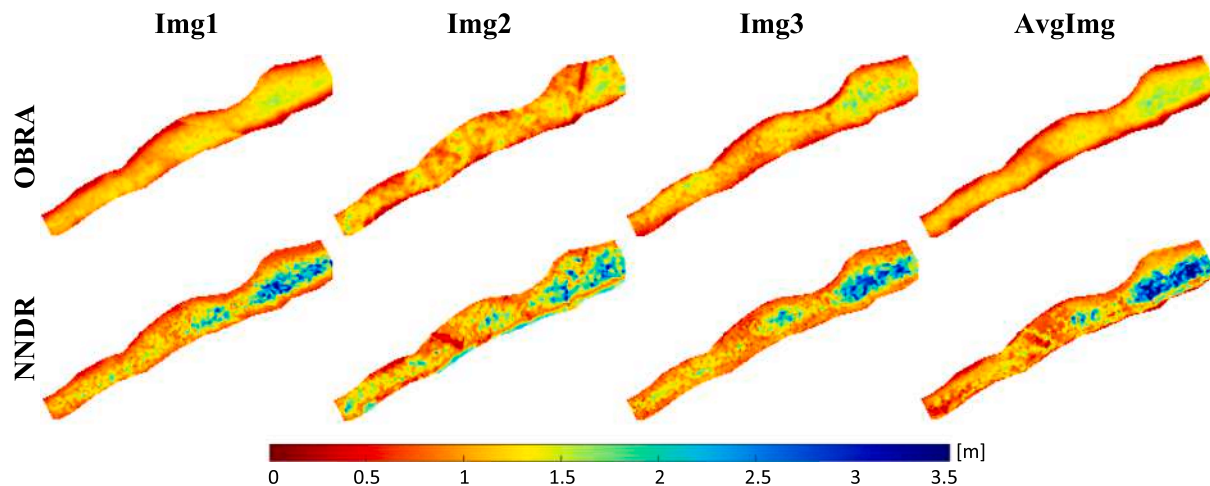


**Fig. 13.** Bathymetry maps derived from single (Img1, Img2, and Img3) and time-averaged (AvgImg) images based on OBRA and NNDR for the American River.

#### 4. Experimental results

This section presents results summarizing the bathymetry via the NNDR and OBRA methods when applied to both single and time-averaged images. For brevity, all of the figures are based on TOA data. However, the accuracy statistics reported in the tables are based on both TOA and BOA data, which allows us to assess the impact of using the atmospherically corrected product. Note that the results are described in greater detail for the first reach (Sacramento River) by providing graphs associated with the training phase of the depth retrieval process. The validation analyses based on in-situ comparisons are presented in detail for all reaches.

##### 4.1. Sacramento River

The OBRA of the time-averaged image for the Sacramento River is shown in Fig. 3a, where the green (545 nm) to red (630 nm) ratio provides the highest  $R^2$  (0.55) among all possible band ratios. The fitted exponential model associated with the optimal band ratio is shown in Fig. 3b.

The training phase of the proposed NNDR for the time-averaged image is summarized in Fig. 4. The comparison analyses for the training and test samples indicate a relatively strong relationship between the image-derived and in-situ depths ( $R^2 > 0.7$ ). Fig. 4c illustrates the performance of NNDR at different training epochs in terms of the mean squared error; the stop criterion is met at epoch 32.

The accuracy of depth retrieval from either single or time-averaged images was assessed based on validation samples that were not used during the training phase. Fig. 5 shows the matchup validations of OBRA and NNDR applied to single and time-averaged images. The bathymetry

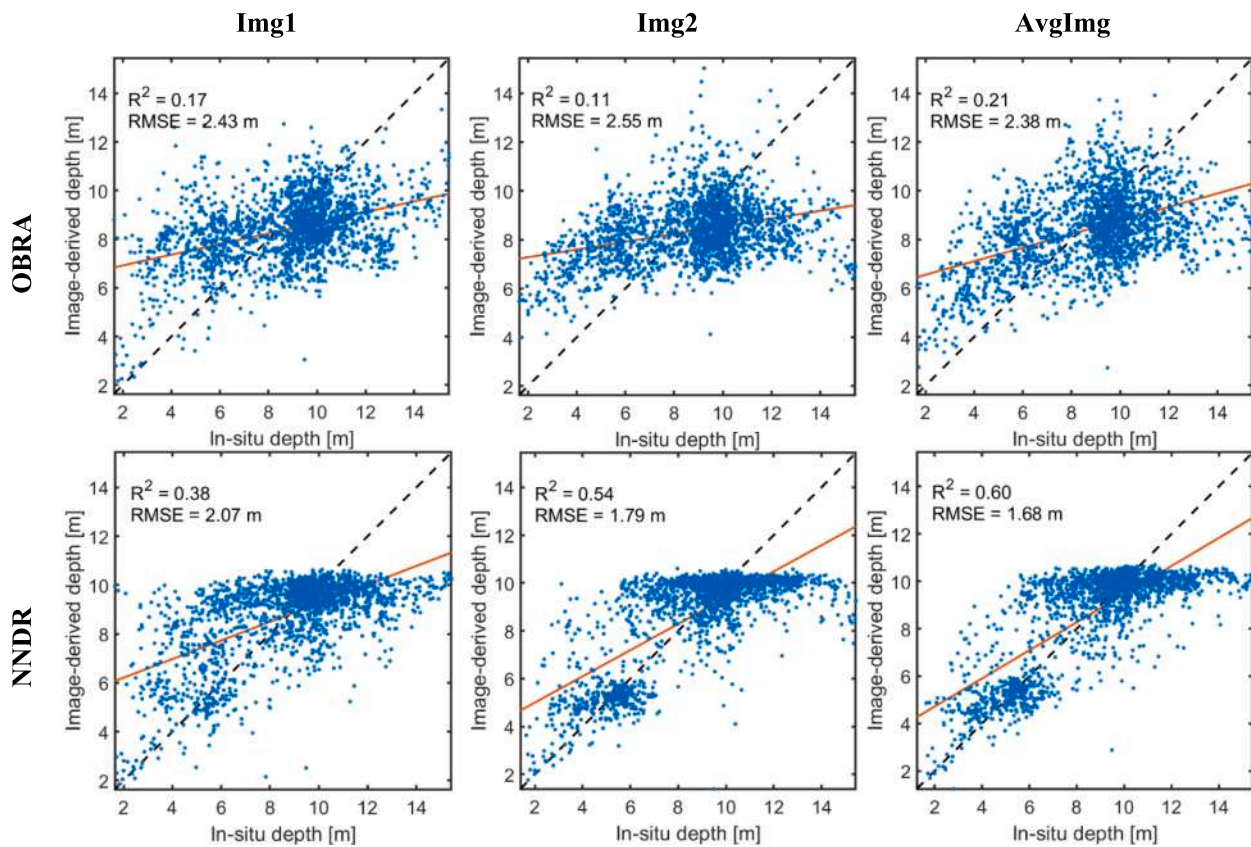


Fig. 14. Validation comparisons of depth retrieval from single (Img1 and Img2) and time-averaged (AvgImg) images based on OBRA and NNDR for the Kootenai River.

Table 5

Accuracy statistics of bathymetry retrieval based on OBRA and NNDR considering TOA and BOA single (Img1 and Img2) and time-averaged (AvgImg) images for the Kootenai River. The best performances are indicated by bold font.

		Img1		Img2		AvgImg	
		OBRA	NNDR	OBRA	NNDR	OBRA	NNDR
R <sup>2</sup>	TOA	0.17	0.38	0.11	0.54	0.21	<b>0.60</b>
	BOA	0.16	0.29	0.14	0.51	0.23	<b>0.57</b>
RMSE [m]	TOA	2.43	2.07	2.55	1.79	2.38	<b>1.68</b>
	BOA	2.45	2.22	2.51	1.84	2.35	<b>1.74</b>
NRMSE [%]	TOA	16	14	17	12	16	<b>11</b>
	BOA	16	15	17	12	16	<b>12</b>
MAE	TOA	1.28	1.22	1.30	1.17	1.27	<b>1.16</b>
	BOA	1.28	1.24	1.29	1.18	1.26	<b>1.17</b>
Bias	TOA	1.01	1.04	0.99	1.02	<b>1.00</b>	1.01
	BOA	1.02	1.05	1.02	1.03	<b>1.01</b>	1.02

retrieval for both OBRA and NNDR improved when using the time-averaged image instead of the single images. For example, NNDR-based R<sup>2</sup> improved by 0.08 and 0.13 when using the time-averaged image compared to single images 1 and 2, respectively. The analyses also reveal that NNDR-based retrievals of bathymetry are more accurate than those of OBRA. For example, NNDR yielded an improvement of 0.19 in R<sup>2</sup> and 0.10 m in RMSE relative to OBRA when using the time-averaged image.

More extensive accuracy statistics are provided in Table 2 for both TOA and BOA data. The time-averaged image consistently enhanced bathymetry estimation compared to the single image retrievals, as indicated by the improved R<sup>2</sup> and RMSE for both TOA and BOA data. MAE also slightly improved for the time-averaged image for depth retrieval based on either OBRA or NNDR. None of the cases resulted in a

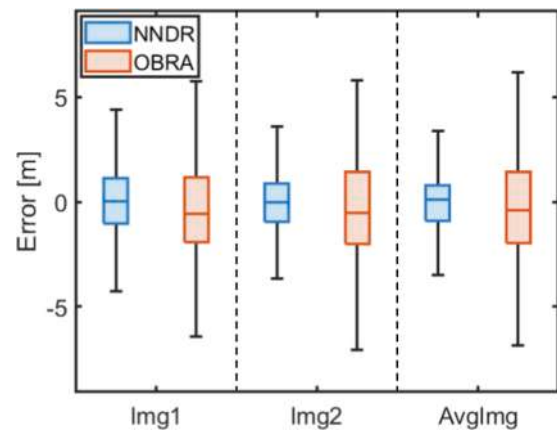


Fig. 15. Errors of bathymetry retrieval from single (Img1 and Img2) and time-averaged (AvgImg) images based on OBRA and NNDR for the Kootenai River.

significant bias, as the bias values were very close to one. Employing BOA data rather than TOA data slightly improved the retrievals based on OBRA. For the time-averaged image, R<sup>2</sup> and RMSE of OBRA improved on the order of 0.1 and 0.04 m, respectively, when using BOA data instead of TOA. However, NNDR-based retrievals were unaffected by changing the image data type from TOA to BOA. This result suggests that NNDR is robust to atmospheric effects, which is consistent with other studies based on machine learning (Duan et al., 2022; Sagawa et al., 2019). The NNDR-based retrieval based on the time-averaged image provides the best NRMSE (9 %).

Distributions of the errors (image-derived values – in-situ values) in bathymetry retrievals are illustrated by boxplots (Fig. 6). The bottom



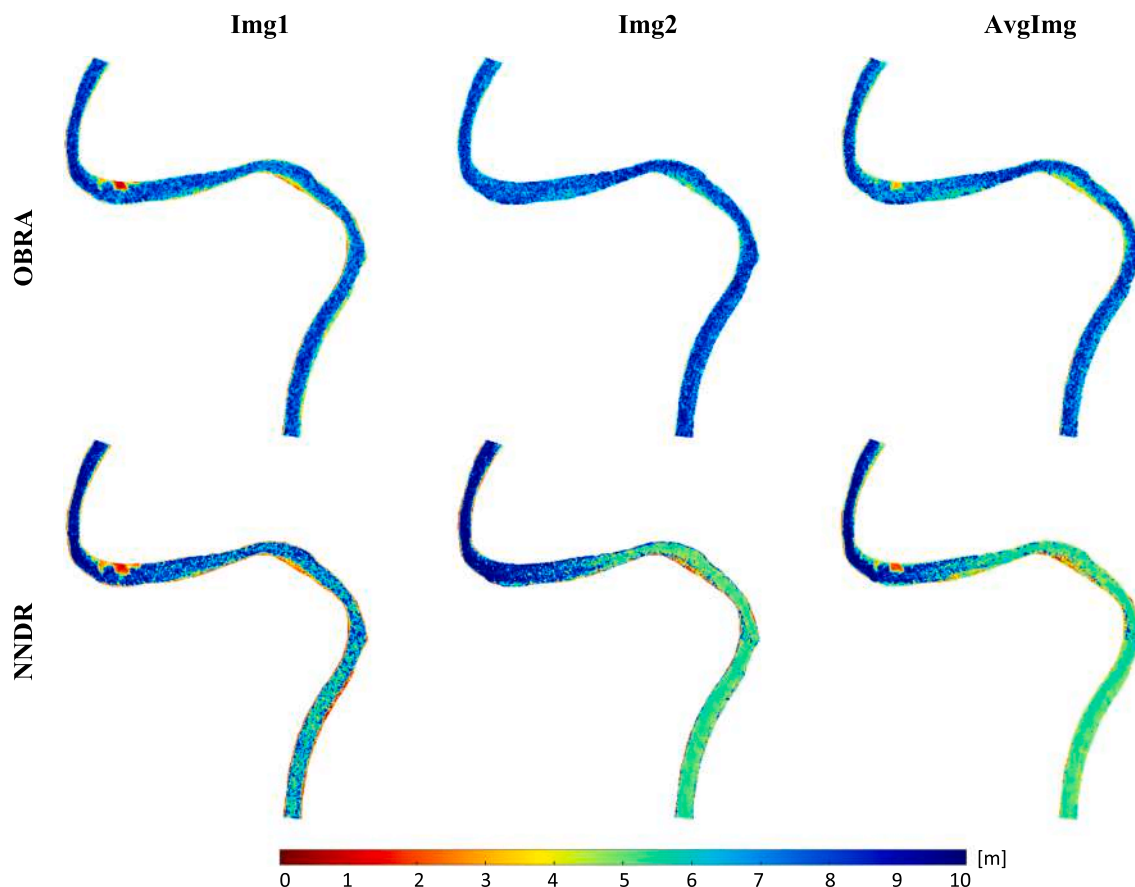


Fig. 16. Bathymetry maps derived from single (Img1 and Img2) and time-averaged (AvgImg) images based on OBRA and NNDR for the Kootenai River.

and top edges of the boxes show the 25th and 75th percentiles, the central marks indicate the median values, and the whiskers show the most extreme errors. The boxes associated with the OBRA-based retrievals are longer and have wider whiskers that indicate larger errors than those from NNDR. The errors associated with the time-averaged image result in smaller boxes with narrower whiskers that indicate the effectiveness of the time-averaging ensemble of short time lag imagery for depth retrieval.

The bathymetry maps derived from single and time-averaged images are shown in Fig. 7. NNDR-based retrievals from the time-averaged image captured deeper waters (>2.5 m), which improved the agreement with in situ observations as indicated in the comparison plots (Fig. 5).

#### 4.2. Salcha River

The comparison plots shown in Fig. 8 indicate an improved NNDR-based bathymetry retrieval when using the time-averaged image instead of single images. The  $R^2$  improvements were 0.09 and 0.17 compared to Img1 and Img2, respectively. The performance of OBRA-based bathymetry retrieval deteriorated slightly when using the time-averaged image. The retrievals of NNDR were more accurate than those of OBRA in all cases. The highest accuracy was achieved by NNDR from the time-averaged image, with an  $R^2$  0.15 higher than the best result achieved from OBRA.

The detailed accuracy statistics for bathymetry retrieval from both TOA and BOA data are given in Table 3. BOA data led to some improvement in the OBRA results, particularly for the time-averaged image, for which the  $R^2$  increased from 0.29 to 0.43. The results of NNDR were less affected by the type of image product (e.g.,  $R^2$  of 0.52 vs 0.50 for TOA and BOA data, respectively). The time-averaged image

enhanced bathymetry retrieval based on NNDR using either BOA or TOA data. OBRA-based bathymetry retrieval from the time-averaged image of the BOA data provided more accurate results than Img2, whereas it was comparable to the results from Img1.

The error boxplots also indicate the effectiveness of image-averaging for depth retrieval and confirm the superior performance of NNDR compared to OBRA (Fig. 9).

The bathymetry maps derived from single and time-averaged images are shown in Fig. 10. In addition to the quantitative assessments provided above, visual inspection of bathymetry maps revealed that the map derived from the time-averaged image was smoother, with a noticeable reduction in pixelated noise.

#### 4.3. American River

Validation comparisons are provided in Fig. 11 for the American River study reach. The image averaging approach again improved depth retrieval compared to single image analyses. The improvements are substantial (e.g., NNDR-based improvement of  $R^2$  and RMSE on the order of 0.4 and 0.24 m compared to Img2). NNDR once again outperformed OBRA with, for instance,  $R^2$  of 0.65 vs 0.33 and RMSE of 0.51 m vs 0.74 m for the time-averaged image. All OBRA-based depth retrievals suffered from underestimation for depths > 1.5 m. NNDR-based bathymetry estimates from the time-averaged image provided the strongest agreement with field observations across the entire range of depths.

The detailed comparison statistics are provided in Table 4. The accuracy metrics were better for the time-averaged image for both OBRA and NNDR. BOA data yielded some improvements in the OBRA-based depth retrievals, whereas the differences between TOA and BOA results were slight for NNDR.

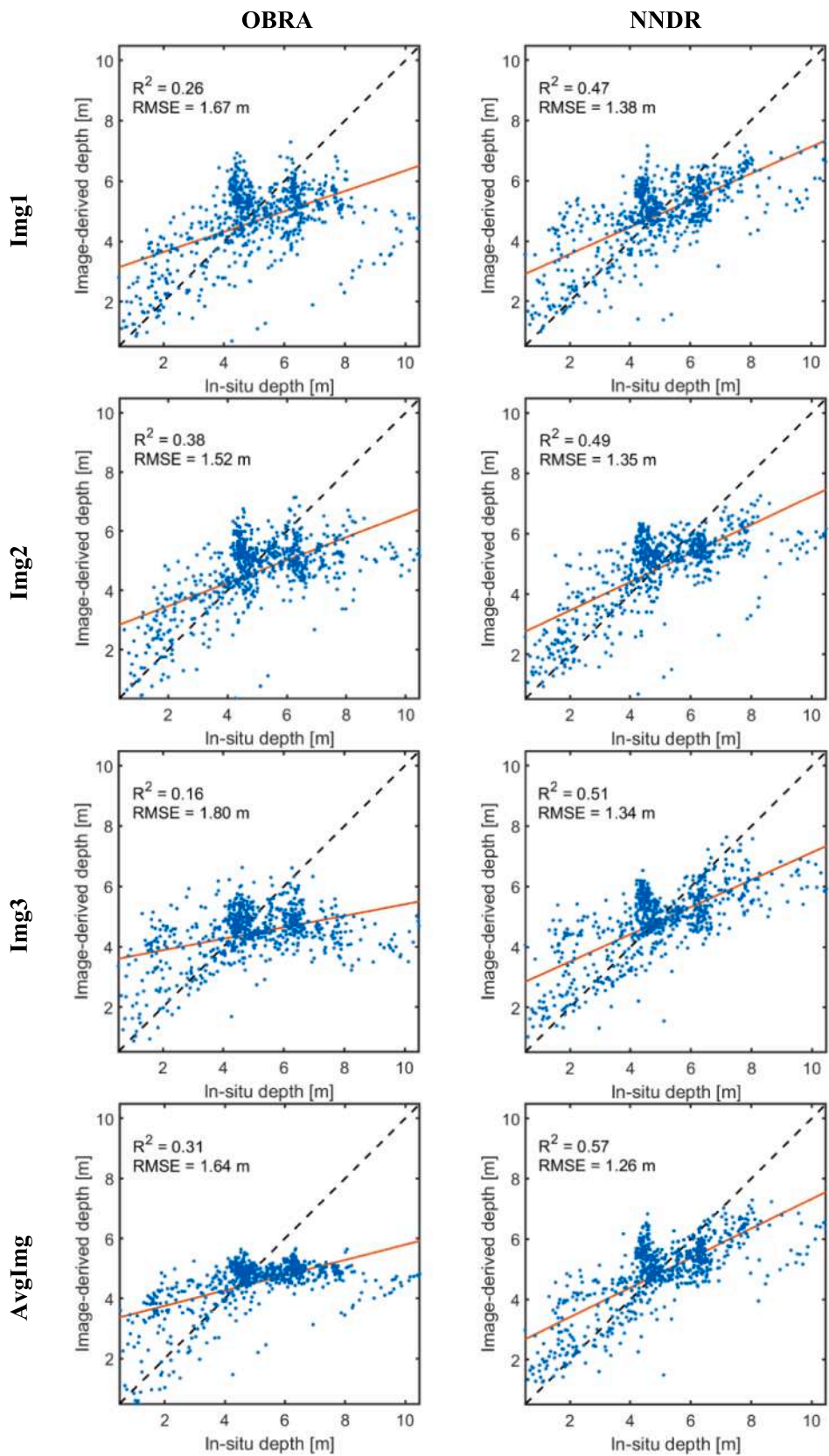
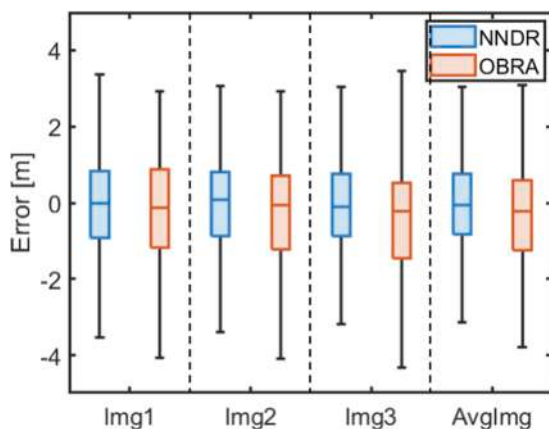


Fig. 17. Matchup validation of depth retrieval from single (Img1, Img2, and Img3) and time-averaged (AvgImg) images based on OBRA and NNDR for the Colorado River.

**Table 6**

Accuracy statistics of bathymetry retrieval based on OBRA and NNDR considering TOA and BOA single (Img1, Img2, and Img3) and time-averaged (AvgImg) images for the Colorado River. The best performances are indicated by bold font.

		Img1		Img2		Img3		AvgImg	
		OBRA	NNDR	OBRA	NNDR	OBRA	NNDR	OBRA	NNDR
$R^2$	TOA	0.26	0.47	0.38	0.49	0.16	0.51	0.31	<b>0.57</b>
	BOA	0.01	0.48	0.06	0.50	0.19	0.53	0.04	<b>0.54</b>
RMSE [m]	TOA	1.67	1.38	1.52	1.35	1.80	1.34	1.64	<b>1.26</b>
	BOA	2.02	1.38	2.01	1.37	1.80	1.31	1.98	<b>1.31</b>
NRMSE [%]	TOA	16	13	14	13	17	13	16	<b>12</b>
	BOA	19	13	19	13	17	12	19	<b>12</b>
MAE	TOA	1.32	1.27	1.29	1.25	1.34	1.26	1.32	<b>1.24</b>
	BOA	1.44	1.28	1.43	1.26	1.39	1.26	1.42	<b>1.25</b>
Bias	TOA	<b>0.98</b>	1.04	0.97	<b>1.02</b>	0.96	1.04	0.97	1.03
	BOA	0.95	1.04	0.93	<b>1.02</b>	0.97	1.04	0.95	1.03



**Fig. 18.** Errors of bathymetry retrieval from single (Img1, Img2, and Img3) and time-averaged (AvgImg) images based on OBRA and NNDR for the Colorado River.

Fig. 12 illustrates the distribution of the depth retrieval errors in the American River. The averaged image resulted in smaller errors than the single images. This case study also confirmed that NNDR-based depth retrieval led to smaller errors than OBRA.

The bathymetric maps also imply that NNDR better resolved the deeper part of the channel, particularly based on the time-averaged image (Fig. 13), which also was evident in the comparison plots (Fig. 11).

#### 4.4. Kootenai River

This case study includes water depths up to 15 m, based on the field measurements, and thus allowed us to assess the potential of PlanetScope imagery and the NNDR technique for mapping bathymetry in not only clear shallow channels but also deeper waters. The validation comparisons imply that time-averaging the image sequences improved depth retrieval (Fig. 14). The  $R^2$  values associated with NNDR estimates are improved by 0.22 and 0.06 compared to the results derived from Img1 and Img2. The associated RMSE improvements were 0.39 m and 0.11 m. OBRA-based retrievals also benefitted from image averaging, but the accuracies remained low ( $R^2 = 0.21$  and  $RMSE = 2.38$  m for the time-averaged image). Although NNDR-based bathymetry retrieval is promising, depths  $> 10$  m were still underestimated. This result was expected because any attempt to map bathymetry from passive optical image data is subject to a maximum detectable depth, which is a function of the optical properties of the water column and the sensor's radiometric characteristics. In essence, light is attenuated exponentially as water depth increases, limiting optically-based depth retrieval even in clear inland water bodies (Legleiter and Fosness, 2019b).

The detailed accuracy statistics derived from in-situ vs image-derived depth comparisons are provided in Table 5. The effect of PlanetScope product level (TOA, BOA) was minimal for bathymetry results derived from either OBRA or NNDR. As in the other case studies, NNDR results were superior compared to OBRA. Note that even though the bias was ideal (equal to 1) for OBRA, this metric only indicates the average bias and in this case, overestimations for shallower waters and underestimation for deeper waters canceled one another. Considering a number of different metrics is important when interpreting the results of any bathymetric mapping exercise.

The distributions of errors also confirm the effectiveness of the proposed image averaging approach for depth retrieval (Fig. 15). The enhanced performance of NNDR compared to the standard OBRA is also evident.

The bathymetry maps derived from single and time-averaged images are shown in Fig. 16. OBRA failed to retrieve the shallower water depths in the southern part of the study area.

#### 4.5. Colorado River

The selected reach of the Colorado River also represented a wide range of bathymetry, with depths up to  $\sim 10$  m. Image averaging appeared beneficial for improving depth retrieval (Fig. 17). The NNDR-based improvements in  $R^2$  were 0.1 and 0.06 with respect to the worst (Img1) and best (Img3) single image results, with associated RMSE improvements of 0.12 m and 0.08 m. NNDR again outperformed OBRA (e.g.,  $R^2$  of 0.57 vs 0.31 for the time-averaged image). Depth retrieval in deep waters appeared challenging, particularly for OBRA. NNDR-based retrievals suffer from underestimation for depth  $> 8$  m.

The accuracy statistics are summarized in Table 6. The time-averaged image again showed strong potential for improving bathymetry estimates. Another key point is that the OBRA-based results based on BOA data were weak ( $R^2 < 0.1$  for two single images), whereas NNDR was minimally affected by the PlanetScope data product type.

The boxplots for NNDR-based retrievals are more compressed than OBRA, indicating smaller estimation errors (Fig. 18). Image averaging also reduced the depth retrieval errors compared to the single images.

Bathymetric maps derived from time-averaged and single images are presented in Fig. 19. OBRA-based depths were underestimated to a greater degree than for NNDR, particularly in the deeper parts of the channel. The pronounced underestimation problem of OBRA was also evident in the validation comparisons (Fig. 17).

## 5. Discussion

The proposed approach built upon averaging image sequences acquired by CubeSats improved bathymetry retrieval using both OBRA and NNDR. Fig. 20 summarizes the improvement percentages (minimum, maximum, and average) in terms of  $R^2$  and RMSE when employing the time-averaged image instead of single images. In only one



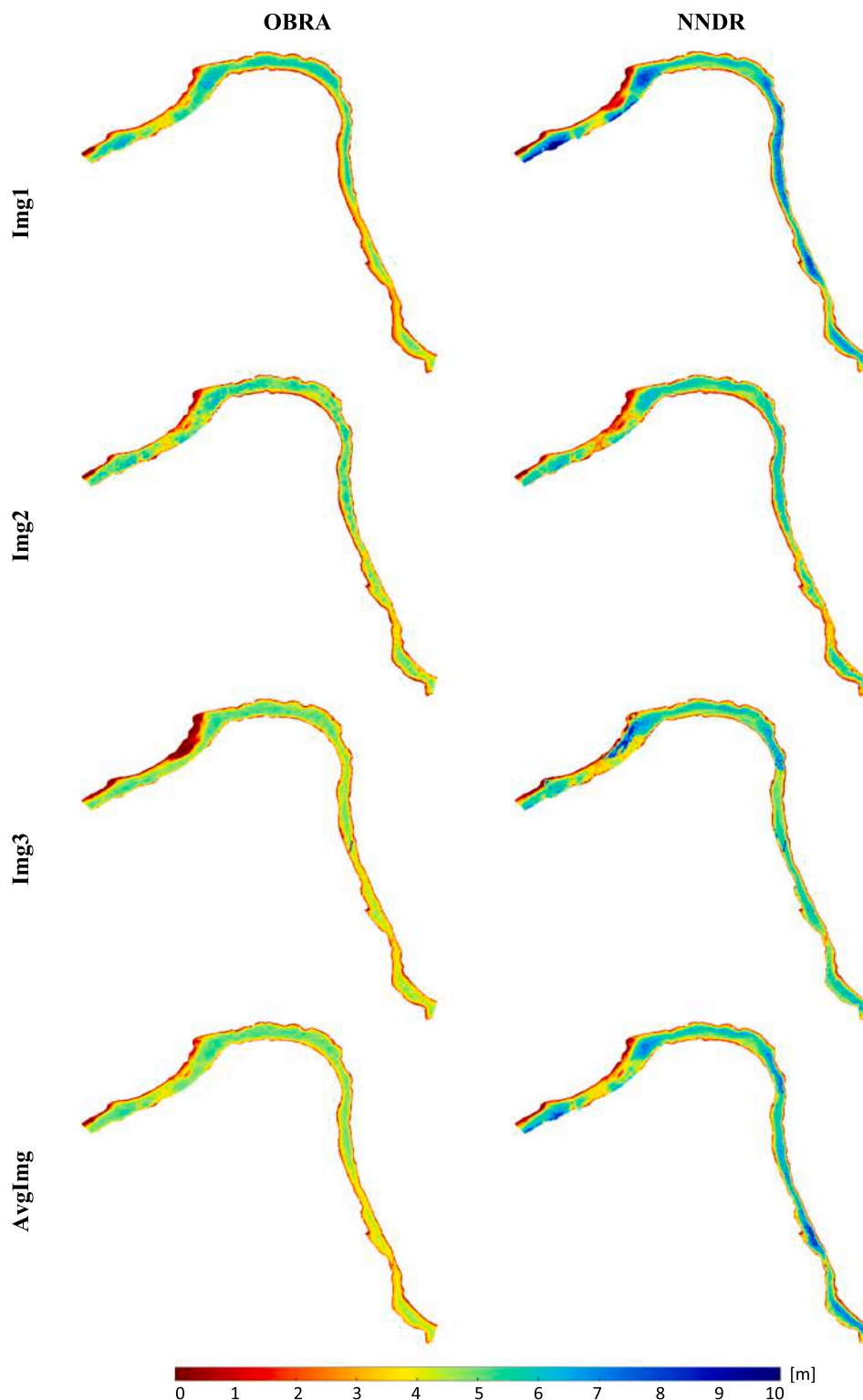


Fig. 19. Bathymetry maps derived from single (Img1, Img2, and Img3) and time-averaged (AvgImg) images based on OBRA and NNDR for the Colorado River.

case, OBRA of the Salcha River, the accuracy decreased when using the time-averaged image. In all other cases, time-averaging led to more reliable depth estimates. The improvements are calculated for each study area and also averaged over the five sites. Depth retrieval from time-averaged images led to 43 % and 35 % improvements of  $R^2$  on average for the five reaches based on OBRA and NNDR, respectively. The RMSE improvements are more pronounced for NNDR-based retrievals than for OBRA (15 % vs 3 % on average). The analyses show that the

highest improvements provided by the image averaging approach were for the American River, based on either OBRA (average  $R^2$  improvement of 117 % and 8 % for RMSE) or NNDR (average  $R^2$  improvement of 73 % and 22 % for RMSE). These results demonstrate the effectiveness of the proposed ensembling approach in improving bathymetry retrieval from CubeSat imagery. NRMSE improved similarly to RMSE when using time-averaged images rather than single frames. However, the key point is that NRMSE remains consistent across all of our case studies (9 % <

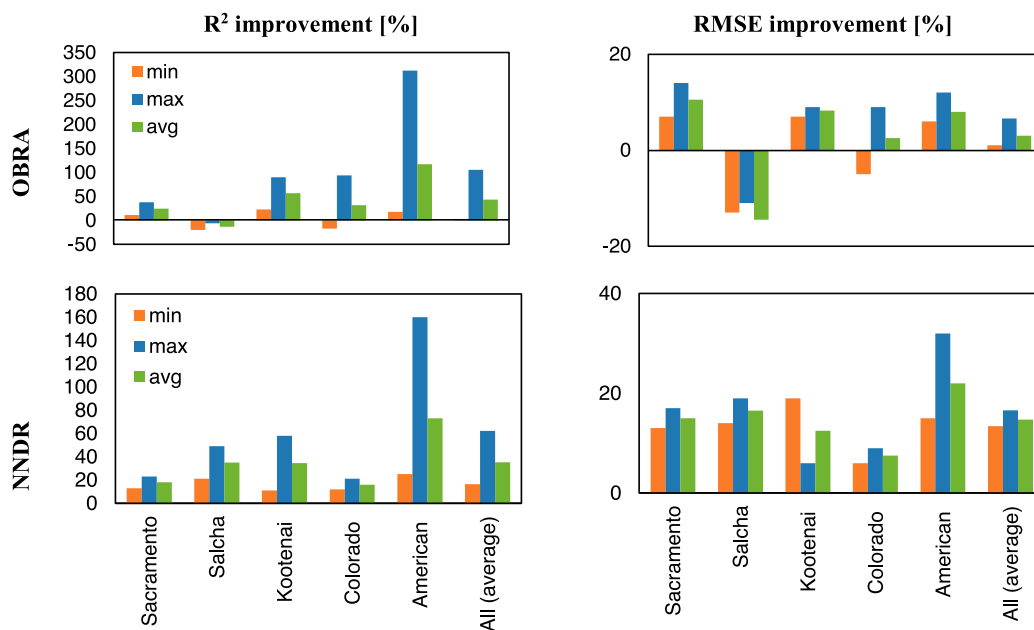


Fig. 20. Improvement percentages of R<sup>2</sup> and RMSE resulting from employing time-averaged images instead of single images for bathymetry retrieval in different river reaches.

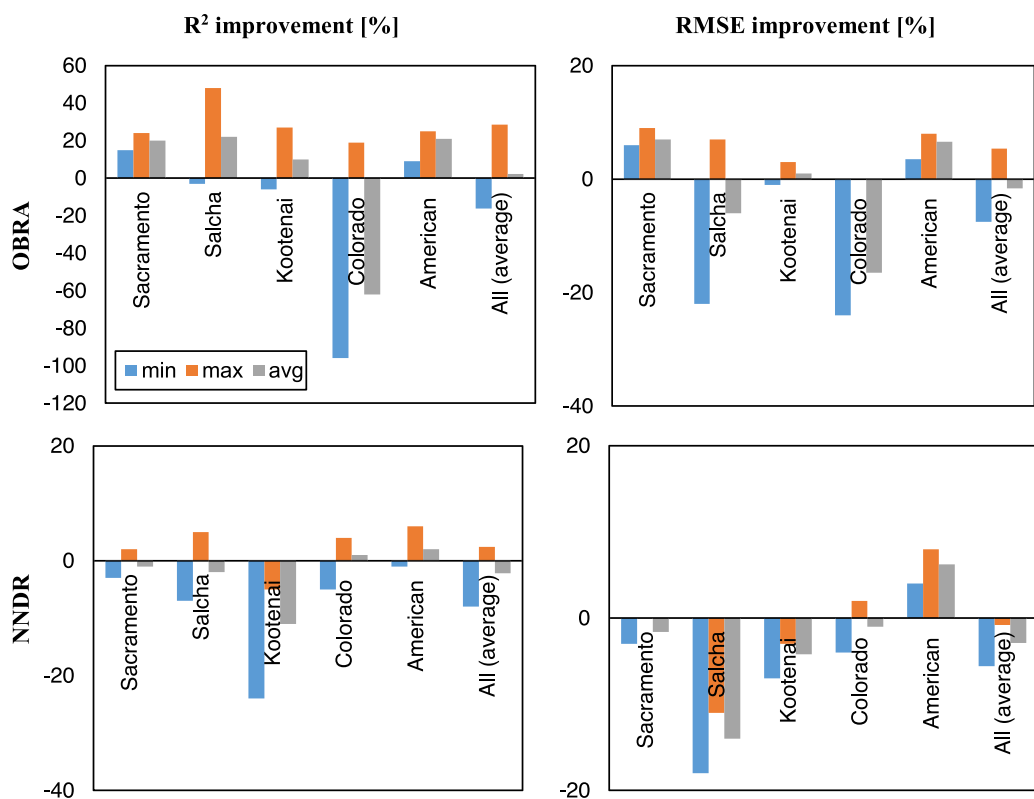


Fig. 21. Improvement percentages of R<sup>2</sup> and RMSE resulting from employing TOA images instead of BOA images for bathymetry retrieval in different river reaches.

NRMSE < 14 %), indicating that the NNDR results in depth retrieval errors that are proportional to the water depth range.

The impact of employing BOA data instead of TOA data is illustrated in Fig. 21 in terms of the R<sup>2</sup> and RMSE improvement percentages. NNDR was less impacted by the image product type. Although BOA data led to some improvements in the OBRA retrievals, the accuracies decreased significantly in some cases (e.g., Colorado River). These results imply

that the PlanetScope BOA product might include sizeable artifacts over water areas that could affect aquatic applications. This finding is consistent with the results of our previous studies (Niroumand-Jadidi et al., 2020b; Niroumand-Jadidi and Bovolo, 2021). Atmospheric correction can mainly be neglected in empirical (regression-based) bathymetry retrieval because actual reflectance values are not as important as they are for physics-based methods (Niroumand-Jadidi et al.,

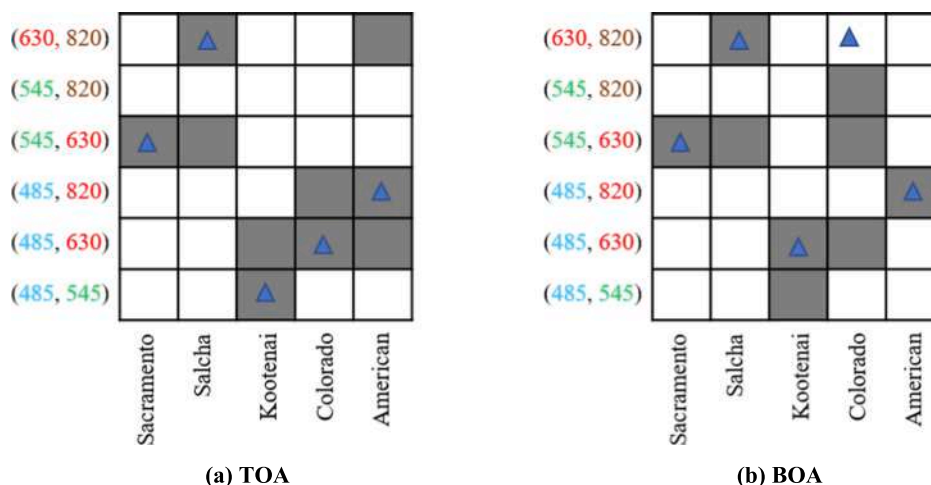


Fig. 22. The optimal pair of bands ( $\lambda_1, \lambda_2$ ) identified by OBRA for different river reaches. The gray-colored cells show the pair of bands for single images, and the blue triangles indicate the ratios for time-averaged images. (For interpretation of the references to color in this figure legend, the reader is referred to the web version of this article.)

2020b). However, if the atmospheric correction is not accurate over aquatic targets, unrealistic alterations of the spectra can lead to uncertainties in depth retrieval, even for empirical methods. Thus, TOA data were preferred over BOA data when applying regression models for bathymetry estimation in our analyses.

Another key finding of our study was the superior performance of NNDR compared to OBRA. Although OBRA identifies the pair of bands providing the strongest correlation with bathymetry through a ratio model, the model itself relies on only a single feature (i.e., band ratio). Under this framework, other spectral bands and features available in the image data are not taken into account. Conversely, NNDR exploits all spectral bands and feature extraction and weighting are handled automatically within the neural network (Murtagh, 1991; Shaheen et al., 2016).

The performance of depth retrieval in shallow rivers indicate slight differences. We suspect that the biases reported for the Salcha River are greater than those for the Sacramento because the Salcha is a smaller river with a greater proportion of mixed pixels that span a range of depths and/or encompass the channel banks. As for the greater improvement associated with time-averaging for the American River, we attribute this result to the fact that three images were available for this site, whereas three of the four other sites had only two images. In addition, the first two images from the American were acquired within half an hour of one another and thus captured conditions that were presumably nearly identical.

Performing OBRA in different reaches indicates that the optimal pair of bands for depth retrieval can vary from river to river and also among the images of a given reach (Fig. 22). For instance, two different pairs of bands including (545 nm, 630 nm) and (630 nm, 820 nm) were identified by OBRA – the first pair for the single images and the latter pair for the time-averaged image. The OBRA of deep reaches (Kootenai and Colorado) using TOA data always involves the blue band as the numerator because shorter wavelengths in the blue provide the highest penetration in water. Analyzing the BOA data, the green band also shows potential as the numerator in the Colorado River. Although the band pairs were identical for TOA and BOA data in the Sacramento and Salcha rivers, there were differences in other reaches. These observations highlight the importance of performing OBRA on an image-by-image basis because the optimal pair of bands can vary depending on the optical properties of the water body, image acquisition characteristics, and image product type.

## 6. Conclusions and future work

In this study, a unique characteristic of the PlanetScope constellation – the ability to acquire imagery with short time lags – is exploited in the context of bathymetry retrieval. We proposed considering an ensemble mean of CubeSat image sequences rather than a single image analysis for mapping bathymetry (i.e. water depth). The bathymetry retrievals in five different case studies with depths up to 15 m indicate the effectiveness of this approach. We also developed a machine learning-based bathymetry model: neural network-based depth retrieval (NNDR). NNDR outperformed widely used OBRA in mapping bathymetry from either single or time-averaged images. NNDR employs all available spectral bands, whereas OBRA relies on a single band ratio. Furthermore, neural networks are capable of learning informative and robust features from the original data without prior extraction of the features. These characteristics of the NNDR enabled substantial improvements in depth retrieval.

The best bathymetry results were achieved when applying NNDR to the time-averaged images. The number of images incorporated into the ensemble averaging was limited to two or three images in our study. An analysis within the original IBARI study indicated that increasing the number of images can further improve bathymetry retrieval (Legleiter and Kinzel, 2021a). With the growing number of CubeSats, the number of sub-daily revisits that result in images with short time lags is expected to increase, further enhancing the performance of the proposed approach. Moreover, additional Dove images from the days close to image acquisition can be incorporated into the ensemble averaging if the bathymetric conditions remain steady over a longer period. On the other hand, with the next generation of CubeSat constellations like the planned Pelican constellation by Planet Labs (Planet, 2022), the number of sub-daily images will increase substantially (from 12 to 30 daily captures with the Pelican constellation). The proposed approach can benefit from the very dense time-series imagery to be provided by the upcoming constellations.

Our study also serves as a broad assessment of the utility of PlanetScope TOA and BOA data products in bathymetric applications. This study demonstrates the potential of Dove imagery for retrieving water depths up to 10 m in the fluvial settings we analyzed. This range of water depth encompasses many inland and even coastal water bodies. The range of detectable depths could even increase in coastal waters with less optical complexity than inland waters. However, further investigations are required to assess the feasibility of depth retrieval from Dove data across a broader range of bio-optical conditions. Although we tested the proposed method in riverine environments, the technique is



generic and can be applied for bathymetry retrieval in any optically-shallow inland or coastal water body. In addition, a new generation of Planet Doves (called SuperDoves) was recently deployed into orbit, providing enhanced spectral resolution (8 bands) with a similar spatial resolution as the current 4-band Doves. Thus, additional opportunities are expected to open up for studying inland and coastal waters by means of CubeSats. A comprehensive multi-sensor study could yield greater insight regarding the utility of CubeSat imagery in bathymetric mapping compared to aerial and satellite imagery with varying spatial, spectral, and radiometric characteristics. In this study, the NNDR model is trained individually for each river. However, the method has the potential to be trained on a much larger, aggregated data set spanning a broad range of bio-optical conditions, which might lead to a generic model transferable in space and time. Thus, further studies could be devoted to training deep networks employing a large number of samples and thus enhancing the generality of the model.

### CRedit authorship contribution statement

**Milad Niroumand-Jadidi:** Conceptualization, Methodology, Software, Data curation, Validation, Visualization, Writing – original draft, Writing – review & editing. **Carl J. Legleiter:** Conceptualization, Methodology, Software, Data curation, Validation, Visualization, Writing – review & editing. **Francesca Bovolo:** Conceptualization, Writing – review & editing.

### Declaration of Competing Interest

The authors declare that they have no known competing financial interests or personal relationships that could have appeared to influence the work reported in this paper.

### Data availability

The in-situ data are available through the links provided in the manuscript.

### Acknowledgments

The authors would like to appreciate Planet Inc.'s Education and Research Program that provided us with the PlanetScope imagery. Paul Kinzel provided constructive feedback that helped to improve the manuscript. Any use of trade, firm, or product names is for descriptive purposes only and does not imply endorsement by the US Government.

### References

- Cooley, S., Smith, L., Stepan, L., Mascaro, J., 2017. Tracking Dynamic Northern Surface Water Changes with High-Frequency Planet CubeSat Imagery. *Remote Sens.* 9, 1306.
- Dekker, A.G., Phinn, S.R., Anstee, J., Bissett, P., Brando, V.E., Casey, B., Fearnas, P., Hedley, J., Klonowski, W., Lee, Z.P., Lynch, M., Lyons, M., Mobley, C., Roelfsema, C., 2011. Intercomparison of shallow water bathymetry, hydro-optics, and benthos mapping techniques in Australian and Caribbean coastal environments. *Limnol. Oceanogr. Methods* 9, 396–425.
- Duan, Z., Chu, S., Cheng, L., Ji, C., Li, M., Shen, W., 2022. Satellite-derived bathymetry using Landsat-8 and Sentinel-2A images: assessment of atmospheric correction algorithms and depth derivation models in shallow waters. *Opt. Express* 30, 3238–3261.
- Gabr, B., Ahmed, M., Marmoush, Y., 2020. PlanetScope and Landsat 8 Imageries for Bathymetry Mapping. *J. Mar. Sci. Eng.* 8, 143.
- Gege, P., 2014. WASI-2D: A software tool for regionally optimized analysis of imaging spectrometer data from deep and shallow waters. *Comput. Geosci.* 62, 208–215.
- U.S. Geological Survey, 2022. USGS water data for the Nation: U.S. Geological Survey National Water Information System database, accessed [30 June 2022], at <https://doi.org/10.5066/F7P55KJN>.
- Ghuffar, S., 2018. DEM Generation from Multi Satellite PlanetScope Imagery. *Remote Sens.* 2018, Vol. 10, Page 1462 10, 1462.
- Giardino, C., Brando, V.E., Gege, P., Pinnel, N., Hochberg, E., Knaeps, E., Reusen, I., Doerffer, R., Bresciani, M., Braga, F., Foerster, S., Champollion, N., Dekker, A., 2019. Imaging Spectrometry of Inland and Coastal Waters: State of the Art, Achievements and Perspectives. *Surv. Geophys.* 40, 401–429.

- Hodúl, M., Bird, S., Knudby, A., Chénier, R., 2018. Satellite derived photogrammetric bathymetry. *ISPRS J. Photogramm. Remote Sens.* 142, 268–277.
- Houborg, R., McCabe, M., 2016. High-Resolution NDVI from Planet's Constellation of Earth Observing Nano-Satellites: A New Data Source for Precision Agriculture. *Remote Sens.* 8, 768.
- Kääb, A., Altena, B., Mascaro, J., 2019. River-ice and water velocities using the Planet optical cubesat constellation. *Hydrol. Earth Syst. Sci.* 23, 4233–4247.
- Legleiter, C.J., 2021a. The optical river bathymetry toolkit. *River Res. Appl.* 37, 555–568.
- Legleiter, C.J., Fosness, R.L., 2019a. Hyperspectral image data and multibeam echosounder surveys used for bathymetric mapping of the Kootenai River in northern Idaho, September 26–27, 2017. U.S. Geol. Surv. data release. URL <https://doi.org/10.5066/P9K54WDL> (accessed 10.3.21).
- Legleiter, C.J., Fosness, R.L., 2019b. Defining the Limits of Spectrally Based Bathymetric Mapping on a Large River. *Remote Sens.* 2019, Vol. 11, Page 665 11, 665.
- Legleiter, C.J., Harrison, L.R., 2019a. Remote Sensing of River Bathymetry: Evaluating a Range of Sensors, Platforms, and Algorithms on the Upper Sacramento River, California, USA. *Water Resour. Res.* 55, 2142–2169.
- Legleiter, C.J., Harrison, L.R., 2019b. Remotely sensed data and field measurements used for bathymetric mapping of the upper Sacramento River in northern California. U.S. Geol. Surv. data release. URL <https://doi.org/10.5066/F7Q52NZ1>. (accessed 10.3.21).
- Legleiter, C.J., Harrison, L.R., 2022. Field measurements of water depth from the American River near Fair Oaks, CA, October 19–21, 2020. U.S. Geol. Surv. data release. URL <https://doi.org/10.5066/P92PNWES>.
- Legleiter, C. J., Kinzel, P.J., 2021. Improving Remotely Sensed River Bathymetry by Image-Averaging. *Water Resour. Res.* 57, e2020WR028795.
- Legleiter, C. J., Kinzel, P.J., 2021. Field measurements of flow depth and optical image sequences acquired from the Salcha River, Alaska, on July 25, 2019. U.S. Geol. Surv. data release. URL <https://doi.org/10.5066/P9S4T8YM> (accessed 10.3.21).
- Legleiter, C.J., Debenedetto, G.P., Forbes, B., 2021. Field measurements of water depth from the Colorado River near Lees Ferry, AZ, March 16–18, 2021. U.S. Geol. Surv. data release. URL <https://doi.org/doi:10.5066/P9HZL7BZ>.
- Legleiter, C.J., Roberts, D.A., Lawrence, R.L., 2009. Spectrally based remote sensing of river bathymetry. *Earth Surf. Process. Landforms* 34, 1039–1059.
- Legleiter, C.J., Tedesco, M., Smith, L.C., Behar, A.E., Overstreet, B.T., 2014. Mapping the bathymetry of supraglacial lakes and streams on the Greenland ice sheet using field measurements and high-resolution satellite images. *Cryosphere* 8, 215–228.
- Li, J., Knapp, D.E., Schill, S.R., Roelfsema, C., Phinn, S., Silman, M., Mascaro, J., Asner, G.P., 2019. Adaptive bathymetry estimation for shallow coastal waters using Planet Dove satellites. *Remote Sens. Environ.* 232, 111302.
- Lyzenga, D.R., 1978. Passive remote sensing techniques for mapping water depth and bottom features. *Appl. Opt.* 17, 379.
- Makboul, O., Negm, A., Mesbah, S., Mohasseb, M., 2017. Performance Assessment of ANN in Estimating Remotely Sensed Extracted Bathymetry. Case Study: Eastern Harbor of Alexandria. *Procedia Eng.* 181, 912–919.
- Mandanici, E., Bitelli, G., 2016. Preliminary Comparison of Sentinel-2 and Landsat 8 Imagery for a Combined Use. *Remote Sens.* 8.
- Mandlbürger, G., Kölle, M., Nübel, H., Soergel, U., 2021. BathyNet: A Deep Neural Network for Water Depth Mapping from Multispectral Aerial Images. *PFG – J. Photogramm. Remote Sens. Geoinf. Sci.* 89, 71–89.
- Mansaray, A.S., Dzialowski, A.R., Martin, M.E., Wagner, K.L., Gholizadeh, H., Stoodley, S.H., 2021. Comparing PlanetScope to Landsat-8 and Sentinel-2 for Sensing Water Quality in Reservoirs in Agricultural Watersheds. *Remote Sens.* 2021, Vol. 13, Page 1847 13, 1847.
- Matlab, 2022. The MathWorks Inc. [Deep Learning Toolbox]. United State, Natick, Massachusetts.
- Mobley, C.D., 1994. Light and water : radiative transfer in natural waters. Academic Press.
- Moses, W.J., Sterckx, S., Montes, M.J., De Keukelaere, L., Knaeps, E., 2017. Atmospheric Correction for Inland Waters. Bio-optical Model. *Remote Sens. Inl. Waters* 69–100.
- Murtagh, F., 1991. Multilayer perceptrons for classification and regression. *Neurocomputing* 2, 183–197.
- Niroumand-Jadidi, M., Bovolo, F., 2021. Water Quality Retrieval and Algal Bloom Detection Using High-Resolution Cubesat Imagery. *ISPRS Ann. Photogramm. Remote Sens. Spat. Inf. Sci.* V-3–2021, 191–195.
- Niroumand-Jadidi, M., Bovolo, F., Bruzzone, L., 2020a. SMART-SDB: Sample-specific multiple band ratio technique for satellite-derived bathymetry. *Remote Sens. Environ.* 251, 112091.
- Niroumand-Jadidi, M., Bovolo, F., Bruzzone, L., Gege, P., 2021. Inter-Comparison of Methods for Chlorophyll-a Retrieval: Sentinel-2 Time-Series Analysis in Italian Lakes. *Remote Sens.* 13, 2381.
- Niroumand-Jadidi, M., Bovolo, F., Bruzzone, L., Gege, P., 2020b. Physics-based Bathymetry and Water Quality Retrieval Using PlanetScope Imagery: Impacts of 2020 COVID-19 Lockdown and 2019 Extreme Flood in the Venice Lagoon. *Remote Sens.* 2020, Vol. 12, Page 2381 12, 2381.
- Niroumand-Jadidi, M., Vitti, A., 2016. Optimal Band Ratio Analysis of Worldview-3 Imagery for Bathymetry of Shallow Rivers (Case Study: Sarca River, Italy). *Int. Arch. Photogramm. Remote Sens. Spat. Inf. Sci.* XLI-B8, 361–364.
- Niroumand-Jadidi, M., Vitti, A., Lyzenga, D.R., 2018. Multiple Optimal Depth Predictors Analysis (MODPA) for river bathymetry: Findings from spectroradiometry, simulations, and satellite imagery. *Remote Sens. Environ.* 218, 132–147.
- Planet Team, 2021. Planet Imagery Product Specifications [WWW Document]. accessed 1.5.21. <https://www.planet.com/products/>.
- Planet, 2022. Pelican | Planet [WWW Document]. accessed 7.1.22. <https://www.planet.com/products/pelican/>.

- Pontoglio, E., Grasso, N., Cagninei, A., Camporeale, C., Dabove, P., Lingua Andrea, M., 2020. Bathymetric Detection of Fluvial Environments through UASs and Machine Learning Systems. *Remote Sens.* 2020, Vol. 12, Page 4148–4148.
- Poursanidis, D., Traganos, D., Chrysoulakis, N., Reinartz, P., 2019. Cubesats Allow High Spatiotemporal Estimates of Satellite-Derived Bathymetry. *Remote Sens.* 11, 1299.
- Roy, D.P., Huang, H., Houborg, R., Martins, V.S., 2021. A global analysis of the temporal availability of PlanetScope high spatial resolution multi-spectral imagery. *Remote Sens. Environ.* 264, 112586.
- Sagawa, T., Yamashita, Y., Okumura, T., Yamanokuchi, T., 2019. Satellite Derived Bathymetry Using Machine Learning and Multi-Temporal Satellite Images. *Remote Sens.* 2019, Vol. 11, Page 1155–1155.
- Salomonson, V. V., Barnes, W., Masuoka, E.J., 2006. Introduction to MODIS and an Overview of Associated Activities. In: Qu, J.J., Gao, W., Kafatos, M., Murphy, R.E., Salomonson, V. V. (Eds.), *Earth Science Satellite Remote Sensing: Vol. 1: Science and Instruments*. Springer Berlin Heidelberg, Berlin, Heidelberg, pp. 12–32.
- Seegers, B.N., Stumpf, R.P., Schaeffer, B.A., Loftin, K.A., Werdell, P.J., 2018. Performance metrics for the assessment of satellite data products: an ocean color case study. *Opt. Express* 26, 7404.
- Shaheen, F., Verma, B., Asafuddoula, M., 2016. Impact of Automatic Feature Extraction in Deep Learning Architecture. 2016. *Int. Conf. Digit. Image Comput. Tech. Appl. DICTA*, p. 2016.
- Shintani, C., Fonstad, M.A., 2017. Comparing remote-sensing techniques collecting bathymetric data from a gravel-bed river. *Int. J. Remote Sens.* 38, 2883–2902.
- Stumpf, R.P., Holderied, K., Sinclair, M., 2003. Determination of water depth with high-resolution satellite imagery over variable bottom types. *Limnol. Oceanogr.* 48, 547–556.
- Toming, K., Kutser, T., Laas, A., Sepp, M., Paavel, B., Nõges, T., 2016. First Experiences in Mapping Lake Water Quality Parameters with Sentinel-2 MSI Imagery. *Remote Sens.* 8, 640.
- Tonion, F., Pirotti, F., Faina, G., Paltrinieri, D., 2020. A Machine Learning Approach to Multispectral Satellite Derived Bathymetry. *ISPRS Ann. Photogramm. Remote Sens. Spat. Inf. Sci.* V-3–2020, 565–570.
- Vanhellemont, Q., 2019. Daily metre-scale mapping of water turbidity using CubeSat imagery. *Opt. Express* 27, A1372.
- Wilson, K.L., Wong, M.C., Devred, E., 2022. Comparing Sentinel-2 and WorldView-3 Imagery for Coastal Bottom Habitat Mapping in Atlantic Canada. *Remote Sens.* 14.